Magmatic Controls on Volcanic Sulfur Emissions at the Iceland Hotspot

E. Ranta[1,2], S. A. Halldórsson[1], B. A. Óladóttir[3], M. A. Pfeffer[3], A. Caracciolo[1], E. Bali[1], G. H. Guðfinnsson[1], M. Kahl[4], and S. Barsotti[3]

[1]Nordic Volcanological Center, Institute of Earth Sciences, University of Iceland, Iceland.

[2]Department of Geosciences and Geography, University of Helsinki, Finland.

[3]Icelandic Meteorological Office, Iceland.

[4]Institut Für Geowissenschaften, Universität Heidelberg, Heidelberg, Germany.

Corresponding author: Eemu Ranta (eemu.ranta@helsinki.fi)

Key Points:

- Volcanic S emission potentials are estimated for 68 Icelandic eruptions using the petrological method.
- Pre-eruptive S contents of Icelandic melts are controlled by sulfide saturation during both melting and crustal magmatic differentiation.
- Icelandic basalts often erupt at compositions close to a maximum in sulfide solubility, leading to relatively high S emission potentials.

Abstract

Outgassing of S (as SO_2) is one of the principal hazards posed by volcanic eruptions. However, S emission potentials of most volcanoes globally are poorly constrained due to a short observational record and an incomplete understanding of the magmatic processes that influence pre-eruptive S concentrations. Here, we use a compilation of published and new data from melt inclusions—which preserve magmatic S concentrations prior to eruptive degassing—from the Iceland hotspot to evaluate the effects of mantle melting and crustal magmatic processes on the S budgets of Icelandic melts. We apply the petrological method to estimate S emission potentials (ΔS_{max}) for 68 eruptions from 22 of the ~33 presently active volcanic systems in Iceland. We show that the S systematics of Icelandic melts are strongly regulated by the sulfide solubility limit. Sulfide-saturated conditions during lower-degree mantle melting, prevalent at off-rift zones, likely explains an observed decoupling between S and Cl. Modelled sulfide solubility peaks in evolved basalts (4-6 wt.% MgO), coinciding with highest melt inclusion S concentrations. Highest ΔS_{max} (2100–2600 ppm) are found in the Hekla 1913 CE, Eldgjá 934 CE and Surtsey 1963-67 CE eruptions in the South Iceland Volcanic Zone. Our results extend the record of volcanic sulfur emissions back in time and can be used to assess volcanic gas hazards at Icelandic volcanoes where no direct measurements are available. Broadly, the results underline the governing role of sulfide solubility during melting and magma differentiation in controlling the eruptible S contents of hotspot magmas.

1 Introduction

Volcanic eruptions release vast quantities of volatiles (H_2O, CO_2, S, Cl and F) into the atmosphere. On geological timescales, volcanic outgassing regulates the composition of Earth's atmosphere (Gaillard et al., 2021). On short timescales, volcanic gases pose one of the principal hazards of eruptions. When gas plumes of large eruptions reach the stratosphere, volcanic sulfur (mainly released as SO_2) forms aerosols that block sunlight and cool the surface, with the potential to cause short-term hemispheric or even global climate perturbations (Robock, 2000). In the troposphere, SO_2 reacts with water and oxidizes to form sulfuric acid and sulfate (SO_4^{-2}) aerosols, with both the gas and aerosol contributing to volcanic pollution that is one of the main environmental and health hazards for eruptions of all sizes (Schmidt et al., 2011; Oppenheimer et al., 2011; Gíslason et al., 2015; Carlsen et al., 2021; Stewart et al., 2021; Ilyinskaya et al., 2017; Stefánsson et al., 2017). Assessing the sulfur release potential of future eruptions based on knowledge from past eruptions is a critical component of both long and short term hazard assessments.

Volatiles in volcanic gas plumes can be measured by satellite instruments (e.g., Schmidt et al., 2015; Carn et al., 2017; Carboni et al., 2019; Esse et al., 2023) or by ground-based measurements (e.g., Vignelles et al., 2016; Ilyinskaya et al., 2017; Pfeffer et al., 2018, *submitted*; Kern et al., 2020; Donovan et al., 2023, Scott et al., 2023). However, direct measurements are only available for a relatively small selection of post-1970's eruptions globally and in Iceland (Oppenheimer et al., 2011). Volatile emissions from past eruptions can be gauged retroactively by indirect means. The 'petrological method' (Anderson, 1974; Devine et al., 1984) utilizes the capacity of crystal-hosted silicate glass melt inclusions (MIs) to retain high volatile concentrations, which in the right circumstances indicate the undegassed, pre-eruptive state of their host magmas (Lowenstern & Thompson, 1995). The key advantage of the petrological method is that volatile emissions from any past eruption where glassy melt inclusions are preserved can be estimated.

The petrological method has been previously applied for a selection of historical and recent Icelandic eruptions (Sigurdsson, 1982; Óskarsson et al., 1984; Devine et al., 1984; Palais & Sigurdsson, 1989; Métrich et al., 1991; Thordarson et al., 1996, 2001, 2003; Sigmarsson et al., 2013; Hartley et al., 2014; Haddadi et al., 2017; Bali et al., 2018, Caracciolo et al., 2023b). These studies reveal the massive atmospheric SO_2 loading resulting from large historical basaltic fissure eruptions in Iceland, exemplified by the Eldgjá 934 CE (~200 Mt SO_2; Palais & Sigurdsson, 1989; Thordarson et al., 2001) and Laki 1783 CE fires (~120 Mt SO_2; Sigurdsson, 1982; Óskarsson et al., 1984; Thordarson et al., 1996). The good accuracy of the petrological method for Icelandic eruptions has more recently been confirmed by excellent match with ground-based SO_2 measurements (Bali et al., 2018; Pfeffer et al., 2018; Pfeffer et al., *submitted*).

However, the volatile emission potentials of most of the 33 active volcanoes in Iceland (www.icelandicvolcanos.is) remain undetermined, leaving a large gap in our understanding of regional volatile systematics and limiting the ability to prepare for future volcanic degassing hazards. Furthermore, effects of petrological processes that determine pre-eruptive S contents, i.e., mantle melting dynamics, mantle source heterogeneity and S concentration, and timing of sulfide saturation during crustal magma evolution are incompletely understood for Icelandic magmas. For example, chalcophile and platinum group element systematics of Icelandic lavas (Momme et al., 2003), along with partial melting models (Ding and Dasgupta 2018) suggest that mantle melting at rift zones is likely sulfide-undersaturated, but that rift melts reach sulfide saturation during crustal evolution (Momme et al., 2003; Halldórsson et al., 2018; Ranta et al., 2022). However, these results are based on limited datasets and are ambiguous with regards to the timing of sulfide saturation and the topology of the sulfide saturation surface ('sulfur content at sulfide saturation' = SCSS; e.g., Shima & Naldrett, 1975; O'Neill & Mavrogenes, 2002; Smythe et al., 2017; Nash et al., 2019; O'Neill, 2021; Ding et al., 2023; Hughes et al., 2023) in the P-T-X space. The SCSS, in turn, essentially controls the theoretical maximum eruptible S concentrations in melts where dissolved S species are dominated by S^{2-} over S^{6+} (Ding et al., 2023; Hughes et al., 2023) such as those in Iceland (Ranta et al., 2022).

Here, we present a database of MI and matrix glass volatile concentrations from 79 Icelandic eruptions, compiled from published data as well as new data from 8 eruptions. We use the database to review the pre-eruptive sulfur systematics of Icelandic volcanoes, from mantle melting to crustal sulfide melt immiscibility, and produce eruption-specific sulfur emission estimates, using the petrological method, for 68 eruptions. Our results can be used to inform forecasts of hazards for future eruptions. For example, an estimate of the S emission potential for a given volcano/volcanic scenario combined with an estimate of effusion rates and injection heights can be used as input data for gas dispersal models in pre-eruptive or early-eruptive phases (Barsotti, 2020), most importantly at volcanoes where no prior direct measurements are available.

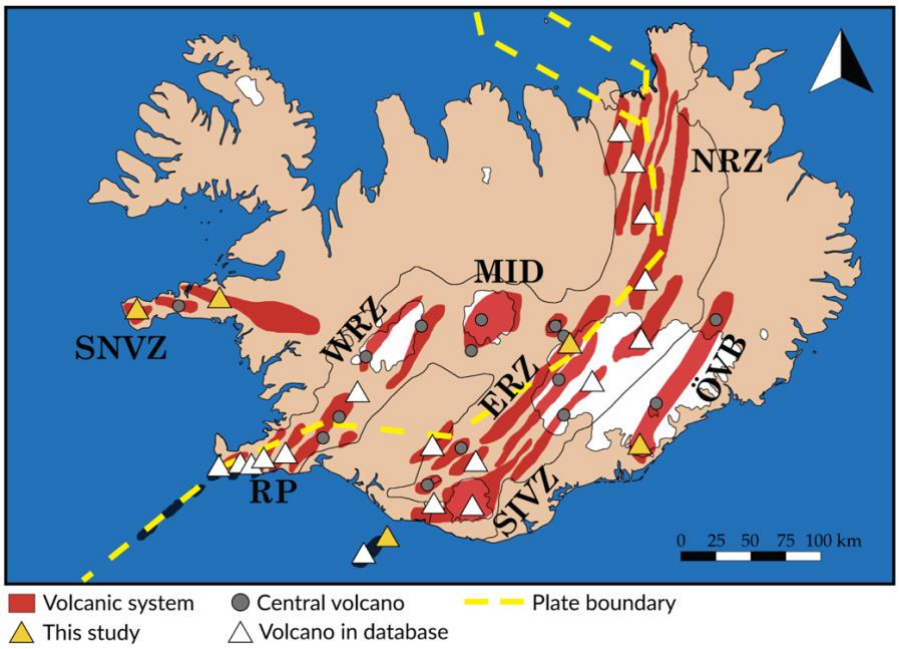

Figure 1. Map of Icelandic neovolcanic zones and volcanic systems (after Jóhannesson & Sæmundsson, 1998). Volcanoes included in the *Iceland melt inclusion catalogue* are shown as triangles, with previously-published data in white and new data in yellow.

2 Geological setting

Iceland is an atypically volcanically active subaerial segment of the slow-spreading Mid-Atlantic Ridge, an ocean island hotspot located at the divergent plate boundary between North America and Eurasia (Fig. 1). Excess magmatism is caused by interaction between the spreading center and a hot mantle upwelling, the Iceland mantle plume (e.g., Schilling, 1973; Ito et al., 1996; Wolfe et al., 1997; Shorttle et al., 2014). At present, 33 volcanic systems in Iceland are considered active, with a collective average eruption interval of 4-5 years (Thordarson & Larsen, 2007; www.icelandicvolcanos.is). The activity is concentrated in several rift segments, here divided into the Eastern, Northern and Western Rift Zones (ERZ, NRZ and WRZ) and the Reykjanes Peninsula (RP), the transform Mid-Iceland Belt (MIB), the propagating rift South Iceland Volcanic Zone (SIVZ) and two off-rift zones, Snæfellsnes Volcanic Zone (SNVZ) and Öræfajökull Volcanic Belt (ÖVB) (Fig. 1). Holocene eruption types vary from common effusive basaltic fissure eruptions (which may have explosive phases) to less frequent explosive silicic eruptions (Thordarson & Larsen, 2007). Many volcanoes are located entirely or partly beneath glaciers; subglacial eruptions are often associated with a major explosive component (Larsen, 2002). Silicic volcanics constitute about 10% of the exposed bedrock (Jónasson, 2007).

3 Methods and catalogue information

3.1 Samples and electron probe microanalysis

New major element and S and Cl concentration data for glassy melt inclusions (hosted in olivine, plagioclase and clinopyroxene) and matrix glasses are presented here from 8 eruptions from 5 volcanoes (yellow triangles in Fig. 1). Seven of these, from the SIVZ, SNVZ and ÖVB were targeted specifically to patch a shortage of S data from these volcanic zones. (1) Fjallsendahraun (~1362 CE;

also known as Frambruni) belongs to the Bárðarbunga volcanic system (Sigmarsson & Halldórsson, 2015; Þórðardóttir, 2020) and is one of the largest Holocene fissure eruptions in Iceland. It is a tholeiitic lava flow with an estimated volume of ~4 km^3 (Thordarson & Larsen, 2007). Two scoria samples from two different craters from the eruptive fissure were used in this study. (2) An unnamed Holocene trachybasalt lava at Djúpalónssandur in the SNVZ from the Snæfellsjökull volcano (Hardarson, 1993). The sample is scoriaceous lava crust. (3) Trachybasalt/basaltic trachyandesite Eldfell eruption that started 23 January 1973 in the island of Heimaey in the SIVZ (Jakobsson et al., 1973; Furman et al., 1991). Two tephra samples were used; ELD-2 is from the first day of eruption (January 23) and ELD-1 was collected from a 'vagabond' crater (collapsed piece of a crater transported by a lava flow) formed during a later stage of the eruption. (4) A scoria sample (BFR-1) was collected from one of the craters of the basaltic Grábrókarhraun lava near the village of Bifröst, which is the easternmost Holocene eruption of the SNVZ and thought to originate from the Ljósufjöll volcanic system (Hardarson, 1993). Sulfur and Cl data are also presented for melt inclusions from tephra of the ~4 ka Berserkjahraun eruption of Ljósufjöll, for which major element data were previously reported by Kahl et al. (2021). (5) Two basaltic (ÖRA-1 and ÖRA-3) and one basaltic trachyandesite lava (ÖRA-2) of unknown age from Öræfajökull were collected from separate stratigraphic units by the Svínafellsjökull glacier (Helgason, 2000). The lavas have a thick (> 1 cm) glassy crust and likely erupted subglacially.

Major element, S and Cl analyses were performed on hand-picked glasses and crystals by electron probe microanalysis (EPMA) with the JEOL JXA-8230 SuperProbe at the Institute of Earth Sciences, University of Iceland, which is equipped with five wavelength-dispersive spectrometers. The analytical settings were identical to those described in Caracciolo et al. (2020) and Ranta et al. (2022). Accuracy of the EPMA measurements and instrumental drift was monitored by analyzing the basaltic glass standard VG-A99 and a Lipari obsidian at the beginning and end of each session. The VG-A99 values for S (137±27 ppm) and Cl (196±22 ppm; both 1σ, n = 12) agree within mutual uncertainty at 1σ level with published values (Supplementary Table 7).

3.2 Compilation of published data

The Iceland Melt Inclusion Catalogue (IMIC; Supplementary Table 1) was compiled from published geochemical melt inclusion (MI) data from Icelandic eruptions. The catalogue includes, to the authors' best knowledge, all MI datasets published at the time of writing (n = 38; references are provided in Table 1) that include measurements of one or more of the five major volatile elements in silicate melts: H (here given as H_2O), C (given as CO_2), F, S and Cl, or B. Where available, associated matrix glass analyses of the host lavas are also included in the database.

3.3 Coverage

IMIC contains a total of 4809 data points from 79 eruptions from 22 volcanic systems. The data are categorized as melt inclusions (n = 2911), matrix glasses (n = 1836), subglacial pillow rim glasses (n = 15) or embayments (n = 40). The data cover all volcanic zones of Iceland, namely the Eastern, Northern and Western Rift Zones (ERZ, NRZ and WRZ), the Reykjanes Peninsula (RP), the propagating rift South Iceland Volcanic Zone (SIVZ) and the two off-rift Snæfellsnes Volcanic Zone (SNVZ) and Öræfajökull Volcanic Belt (ÖVB) (Fig. 1). Compositionally, 84.4% of the analyses are basaltic (SiO_2 < 52 wt.%), 14.2% are silicic (SiO_2 > 65 wt.%), and 1.4% intermediate (SiO_2 = 52-65 wt.%) (Fig. 2). Of the volcanic zones, the SNVZ, ÖVB and WRZ have the poorest coverage with each constituting less than 4% of the total, whereas data from the main active rift zones ERZ, NRZ

and RP together contribute about 86% of the total. The individual volcanoes with most MI data are Bárðarbunga (n = 517), Grímsvötn (n = 401) and Fagradalsfjall (n = 232) (Fig. 3).

3.4 Data type, quality and filtering

Volatile concentrations in volcanic glasses are typically determined using microanalytical techniques that enable the analysis of melt inclusions as small as ~5 μm in diameter. The most common analytical techniques are secondary ion mass spectrometry (SIMS; H_2O, CO_2, F, S, Cl), electron probe microanalysis (EPMA; F, S, Cl), Fourier transform infrared spectroscopy (FTIR; H_2O, CO_2) and Raman spectroscopy (H_2O, CO_2). Data from all these techniques are represented in IMIC, and the methods used by each study are specified in Table 1. To retain the data integrity, no filtering was done, and published data are reported in IMIC as in the original publications. However, volatile concentrations reported for MIs that have been rehomogenized under atmospheric pressure are considered unreliable due to possible volatile loss during reheating (Caracciolo et al., 2020, 2022; Venugopal et al., 2020) and are thus not considered further.

Post-entrapment process (PEP) correction. Major and trace element and volatile concentrations in melt inclusions can be modified by post-entrapment crystallization and/or diffusive re-equilibration (e.g., Danyushevsky et al., 2000). PEP can significantly affect the concentrations of compatible elements in the residual melt (e.g., MgO; Fig. S1a) but the effect is minor (< 20%) for incompatible elements, including S (Fig. S1b). Some, but not all, studies perform PEP corrections to reconstruct original melt inclusion compositions. However, the correction schemes vary between studies and depend on the host-crystal. When possible, both the measured concentration data (i.e., prior to PEP corrections) as well as the reported PEP-corrected values are reported in IMIC. Thus, the catalogue user has access to unprocessed data and can opt to make PEP corrections using the method of their choice.

197

Table 1: Inventory

Reference	Volcano[1]	Eruptions	Mafic	Interm.	Silicic	MI	MG	H_2O	CO_2	F	Cl	S	B	Methods
Sigurdsson1982	Grí	Laki 1783 CE				x	x					x		EPMA
Devine1984	Grí, Hei, Hek, Kat, Kra	Multiple	x		x	x	x					x		EPMA
Óskarsson1984	Grí	Laki1783	x			x	x					x		
Palais1989	Kat, Ör	Eldgjá, 1362 CE	x		x							x		EPMA
Métrich1991	Grí	Laki 1783 CE	x			x	x					x		EPMA
Þórðarson1996	Grí	Laki 1783 CE				x	x			x	x	x		EPMA
Þórðarson2001	Kat	Eldgjá	x			x	x					x		EPMA
Þórðarson2003	Bár	Þjórsárhraun										x		EPMA
Moune2007	Hek	1913 CE, 2000 CE	x	x		x	x	x		x	x	x		EPMA, SIMS
Sharma2008	Ör	1362 CE			x	x	x			x	x	x		EPMA
Portnyagin2012	Hek	H3, H4		x	x	x	x	x		x	x	x	x	EPMA, SIMS, FTIR
Moune2012	Eyj	Fimmvörðuháls 2010 CE	x			x		x		x	x	x		EPMA, SIMS
Brounce2012	Grí	Laki 1783 CE	x					x	x	x	x	x	x	SIMS
Owen2013	Tor	Multiple			x	x	x	x			x			SIMS, FTIR
Sigmarsson2013	Grí	Grímsvötn 2011 CE	x			x	x					x		EPMA
Hartley2014	Grí	Laki 1783 CE	x			x	x	x	x					EPMA, SIMS, Raman
Neave2014	Bár	Skuggafjöll	x			x		x	x	x		x		EPMA, SIMS, Raman
Schattel2014	Ask, Ör	1875 CE, 1362 CE			x	x	x	x		x	x	x		EPMA, SIMS, FTIR
Schipper2016	Sur	Surtsey 1963-7 CE	x			x	x	x	x	x	x	x		SIMS
Gauthier2016	Bár	Holuhraun 2014-15 CE	x			x	x			x	x	x		EPMA
Lucic2016	Hek	H3, 1104 CE, 1845 CE, 1991 CE		x	x	x	x	x	x		x	x		EPMA, FTIR
Haddadi2017	Grí	1823 CE, 1873 CE, 2004 CE, 2011 CE	x			x	x	1	1	x	x	x		EPMA
Neave2017a	Grí	Saksunarvatn	x			x	x	x	x	x	x	x	x	EPMA, SIMS
Hauri2018	Þei	Borgarhraun	x			x		x	x	x	x	x		SIMS
Hartley2018	Bár	Holuhraun 2014-15 CE											x	EPMA, SIMS
Bali2018	Bár	Holuhraun 2014-15 CE	x			x	x	x	x	x	x	x		EPMA, SIMS, FTIR, Raman
Liu2018	Kra	Hverfjall	x			x	x	x	x		x	x		FTIR, EPMA
Miller2019	Hen	Miðfell	x			x	x	x	x	x	x	x		EPMA, SIMS
Caracciolo2020	Bár	Multiple	x			x	x				x	x		EPMA, SIMS
Hartley2021	Ask	Multiple	x		x	x	x	x	x	x	x	x	x	EPMA, SIMS, Raman
Matthews2021	Rey, Ljó, Fre	Multiple	x			x	x		x	x	x	x	x	EPMA, SIMS
Rooyakkers2021	Kra	Multiple			x	x	x				x	x		EPMA
Ranta2022	Kve	Multiple	x			x	x	x	x		x	x		EPMA, FTIR
Caracciolo2022	Bár	Multiple	x			x	x				x	x		EPMA
Marshall2022	Bár	Holuhraun 2014-15 CE	x			x	x						x	SIMS
Halldórsson2022	Fag	Fagradalsfjall 2021 CE	x			x	x	x	x		x	x		SIMS, EPMA
Caracciolo2023a,b	Bre, Krý, Rey, Sva	Multiple	x			x	x				x	x		EPMA
This study	Hei, Snæ, Ljó, Bár, Ör	Multiple	x	x		x	x				x	x		EPMA

198
199
200

[1]Ask = Askja; Bár = Bárðarbunga; Bre = Brennisteinsfjöll; ERZ = Eastern Rift Zone (subglacial); Eyj = Eyjafjallajökull, Fag = Fagradalsfjall; Fre = Fremrinámar; Grí = Grímsvötn; Hek = Hekla; Hei = Heimaey; Hen = Hengill, Kat = Katla; Kra = Krafla; Krý = Krýsuvík; Kve = Kverkfjöll; Ljó = Ljósufjöll; Rey = Reykjanes; Snæ = Snæfellsjökull; Sv = Svartsengi; Tor = Torfajökull; Þei = Þeistareykir; Sur = Surtsey; Sva = Svartsengi; Ör = Öræfajökull.

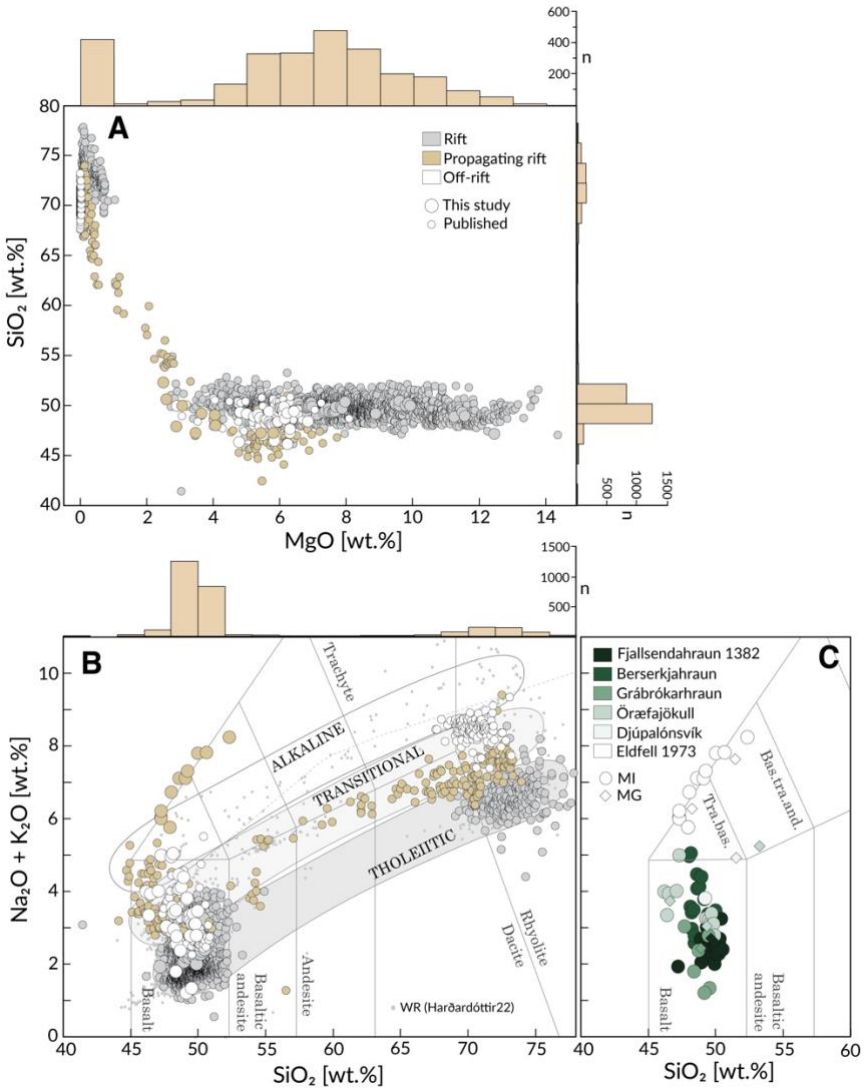

Figure 2. Overview of the Iceland melt inclusion catalogue (IMIC). (a) SiO_2 vs MgO. (b) Total alkali (Na_2O+K_2O) vs SiO_2 (TAS). The A and B panels show published melt inclusion data (matrix glasses, embayments and pillow glasses are omitted). There is a broad overlap of melt inclusions with whole-rock data from Iceland from the compilation of Harðardóttir et al. (2022; grey dots in (b)). Histograms in (a) and (b) highlight that the distribution of the data is heavily skewed toward basaltic compositions. (c) A cropped TAS diagram with a detailed overview of new data. MI = melt inclusion. MG = matrix glass.

3.5 The petrological estimate of eruptive volatile emissions

3.5.1 Calculation of volatile fluxes based on the petrological method

If the pre-eruptive (C_0) and post-eruptive (C_1) volatile concentrations and the crystallinity (X_{cryst}) of a given eruption are known, the eruptive volatile release per unit mass of melt (ΔC, [kg volatile/kg melt]) can be calculated as

$$\Delta C = (1–X_{cryst})(C_0 – C_1) \quad (1)$$

Melt inclusions generally preserve high volatile concentrations that are used as an approximation of the pre-eruptive state (C_0) of a magma. In turn, matrix glasses—which most commonly either quenched rapidly after leaving the vent (tephra) or at the surface of a lava flow (lava crust)—provide an estimate of the post-eruptive volatile contents (C_1). Because the exact crystallinity of lavas is not reported for the majority of the eruptions in IMIC, we opt to use $X_{cryst} = 0$ for all ΔC calculations.

C_0 and C_1 are chosen differently depending on the volatile species. For H_2O, F and Cl, the average MI and matrix glass concentrations are used for C_0 and C_1, respectively. In cases where H_2O was not analyzed in matrix glasses it is assumed that $[H_2O]_1 = 0$, which reflects the low H_2O concentrations in Icelandic bulk lavas and matrix glasses.

For sulfur, S_0 is chosen differently for melt compositions above and below MgO = 4 wt.% because of the pronounced effect of sulfide saturation on S concentrations in melts below that approximate threshold (Ranta et al., 2022; section 5.2). For melt compositions with MgO > 4 wt.%, S_0 is taken as the *highest* measured MI concentration (after discarding outliers, always outside 75% confidence interval) following empirical evidence that this approach leads to close correspondence with observed emissions (Bali et al., 2018; Pfeffer et al., 2018, *submitted*). For melts with MgO < 4 wt.% (low-MgO basalts to rhyolites), S_0 is here instead chosen as the mean MI S content. For all melt compositions, S_1 is chosen as the *minimum* S concentration measured in matrix glasses. The minimum concentration is used due to an analytical bias toward higher concentrations than bulk erupted material, because analyses are generally performed on the fastest quenched glass (and hence least degassed) material. Because S concentrations in tephra glasses from a single eruption may vary depending on how fast the sample was quenched (Sigmarsson et al., 2013; Liu et al., 2018), it is useful to differentiate between the apparent sulfur release at the vent

$$\Delta S_{vent} = S_0 - S_1 \quad (2)$$

and the maximum sulfur emission potential

$$\Delta S_{max} = S_0 \quad (3)$$

which reflects degassing of all pre-eruptive sulfur (i.e., $S_1 = 0$ in eq.2).

If the total dense rock estimate volume, V_{DRE} [m^3] (equivalent of vesicle-free solidified lava), and density, ρ [kg/m^3], of the erupted products are known, the total mass of volatile release, m [kg], can be calculated as

$$m = \Delta C \times \rho \times V_{DRE} \quad (4)$$

The densities (ρ) of the solidified lava and the melt are assumed to be 2710 kg/m^3 for basalts, 2600 kg/m3 for intermediate rocks and 2470 kg/m^3 for silicic rocks (Sharma et al., 2008, Hartley and Maclennan 2018). For tephras with no reported V_{DRE}, we make the approximation

$$V_{DRE} = bV \quad (5)$$

where V is the estimated volume of tephra deposits and/or the lava flow volume and b is a scaling factor that accounts for vesicularity (Table S2).

3.5.2 Caveats and sources of error of the petrological method

Several caveats apply when using the petrological method:

1. Melt inclusions do not always accurately record the volatile composition of the pre-eruptive melt. Volatile concentrations in MIs can strictly represent the pre-eruptive state of the melt *only if* they were trapped from the carrier melt shortly before eruption *and* were quenched rapidly enough to prevent diffusive modifications or post-entrapment crystallization. More commonly, MIs formed during an earlier stage of the magma's history. Then, decoupling of MI and host melt after entrapment partly shields the MI from subsequent magmatic processes (e.g., fractional crystallization, magma recharge, gas fluxing, vapor or sulfide saturation) that may have caused the host magma to either lose or gain volatiles. The common observation that MIs and their host minerals tend to be more primitive and chemically heterogeneous than the carrier melts (e.g., Maclennan, 2008; Thomson & Maclennan, 2013) reflects such decoupling. This problem is partly overcome in our ΔS calculations by the choice of maximum MI S concentration, which is typically found in MIs with MgO contents that closely matches the carrier melt.
2. Different volatile species need to be treated separately because of their differing solubilities and diffusion rates in melts (Baker et al., 2005), and additional factors that affect their concentrations in melts and their preservation in melt inclusions:
3. Accurate CO_2 measurements in MIs are complicated by the necessity to account for vapor bubbles and mineral precipitates on the bubble walls, which can host more than 90% of the CO_2 contained in the MI (Hartley et al., 2014; Moore et al., 2015; Rasmussen et al., 2020; Schiavi et al., 2020), and decrepitation, which leads to loss of CO_2 (Maclennan, 2017). Bubbles in MIs may also host S as gas or precipitates (Venugopal et al., 2020), but the effect on total MI S contents may be insignificant (Rasmussen et al., 2020; Korneeva et al., 2023).
4. Water, due to the high diffusivity of H^+, is especially prone to re-equilibration which can lead to both increased and decreased H_2O contents in the melt inclusion (Hauri et al., 2002; Gaetani et al., 2012; Bucholz et al., 2013; Barth & Plank, 2021). This means that MIs are more likely to have equilibrated with their carrier melts with respect to H_2O, thus representing true pre-eruptive contents, although the same effect can generate artificially low MI H_2O concentrations via post-eruptive re-equilibration with a degassed host melt. Concentrations of F, Cl and S—all slow-diffusing elements relative to H (Freda et al., 2005; Baker et al., 2005)—are here assumed to be only affected by post-entrapment crystallization, which leads to an increase of their concentrations in the residual melt. This distillation effect leads to only a small increase in the measured concentrations (< 5%) for the typically modest (< 15%) reported amounts of post-entrapment crystallization and is always less than 20% for published data (Fig. S1b).
5. A caveat of the previous point is that boundary layer effects during MI entrapment can lead to diffusive fractionation that generate higher concentrations of slow-diffusing elements in the MI relative to the original melt (Baker, 2008). In experiments, MI with S and Cl enrichments of up to 50% and 40%, respectively, have been observed (Baker, 2008).
6. Sulfide globules in MIs may buffer the glass S concentrations. Sulfide globules in Icelandic MIs occur (Ranta et al., 2022) but are relatively rare (observed in less than approximately 2% of basaltic MIs according to the collective experience of the authors). These may either signal trapping of melts that were already sulfide-saturated prior to MI entrapment but could also form post-entrapment if the trapped melt reaches SCSS, for example, by post-entrapment crystallization (Audétat et al., 2018). In the latter case, the measured MI glass S concentration by microanalytical methods would lead to underestimation of the original melt S content. This effect could be overcome by rehomogenization of MIs (Korneeva et al., 2023), or by bulk LA-ICP-MS measurements of MIs (Rottier & Audétat, 2019) in setups where S can be quantitatively determined.
7. The petrological method only takes into account the volatile emission capacity of the erupted melt itself. Actual volcanic volatile emissions may additionally involve input from magmatic S-bearing volatile phases or external sources of volatiles (see section 5.2).

8. The petrological method also neglects post-eruptive outgassing from cooling lava, which is an additional source of volcanic pollution (Óskarsson et al., 1984; Thordarson et al., 1996; Simmons et al., 2017; Pfeffer et al., 2018; Sigmarsson et al., 2020; Donovan et al., 2023). This process disproportionately affects F and Cl, which only reach melt saturation as their concentrations in residual melts are driven up by microlite crystallization in cooling lava fields. Thus, petrological F and Cl emission estimates—often negligible (Fig. S4)—should be taken as minimum values.
9. Slow diffusivity of S in silicate melts may cause disequilibrium degassing (Lerner et al., 2021), which may explain commonly observed matrix glass S contents above the solubility limit of melts at surface pressures. The residual sulfur is progressively degassed from a cooling lava field, as seen in progressively waning S concentrations in matrix glasses with increasing distance to the vent and measurable SO_2 degassing of lava fields observed by field measurements ((Lerner et al., 2021, Donovan et al., 2023). For this reason, we consider ΔS_{max} to be a more reliable indicator of total SO_2 release.

Minding these caveats, the petrological method is broadly considered to be a reliable way to measure pre-eruptive S concentrations (e.g., Devine et al., 1984; Wallace & Edmonds, 2011; Lerner et al., 2021) and has proven to be an accurate means for estimating SO_2 emissions of Icelandic eruptions (Bali et al., 2018; Pfeffer et al., 2018, *submitted*).

4 Results

4.1 New measurements

The new EPMA data include major element compositions of matrix glasses (9 samples from 7 eruptions), melt inclusion glasses (n = 72) and their host crystals, i.e., olivine (n = 28), plagioclase (n = 47) and clinopyroxene (n = 3) (Tables S3-S6). The matrix glasses vary in composition from tholeiitic basalt (Fjallsendahraun; MgO = 6.7 wt.%) to basaltic trachyandesite (Eldfell 1973; Fig. 2c). Of the SNVZ samples, the Djúpalónsvík lava crust has an evolved trachybasaltic composition (MgO = 4.3 wt.%, Na_2O+K_2O = 4.9 wt.%), whereas the Grábrókarhraun and Berserkjahraun tephra glasses are basaltic (MgO of 6.0 and 5.8 wt.%, respectively) and less alkaline (Na_2O+K_2O = 2.4 and 3.7 wt.%, respectively). Two of the Öræfajökull samples (ÖRA-1 and 3) are evolved basalts (MgO = 5.2 and 5.4 wt.%, respectively), and the third (ÖRA-2) is a basaltic trachyandesite (MgO = 2.75 wt.%) but lacks glassy MIs.

Notably, the Eldfell MIs lie outside of the compositional coverage of previously published MI data, being more alkaline and extending from trachybasaltic to basaltic trachyandesitic compositions (the latter exemplified by the ELD-2 tephra glass from 23 January 1973, the first day of the eruption; Fig. 2c). These compositional trends echo the bulk rock compositions of the eruption (Jakobsson et al., 1973; Sigvaldason & Óskarsson, 1976; Furman et al., 1991).

The Fjallsendahraun tephra is very similar in composition to other historic Bárðarbunga eruptions—in particular, with the 2014-2015 Holuhraun eruption (Halldórsson et al., 2018)—and in line with previously reported data (Þórðardóttir, 2020). Sulfur concentrations of Fjallsendahraun MIs can be divided into two groups: lower S contents from 860 to 1050 ppm are measured in a group of high-MgO (9.5–12.5 wt.%) melt inclusions hosted in high-An plagioclase ($An_{87.8–91.1}$), whereas higher S contents between 1200 and 1590 ppm (mean 1395±111 ppm, 1σ, n = 29, excluding a low-S outlier) are seen in remaining MIs which have lower MgO (7.1±0.6 wt.%, 1σ) and are hosted in plagioclase ($An_{81.3–89.3}$), olivine ($Fo_{78.8–84.9}$) and clinopyroxene ($Mg\#_{83.9–85.2}$). The S contents of the high-S MIs are very similar to other published Bárðarbunga MI data (Bali et al., 2018; Caracciolo et al., 2020; Fig. 3).

4.2 Sulfur concentrations of Icelandic melt inclusions

Sulfur concentrations in Icelandic melt inclusions in IMIC vary between 3 and 2630 ppm (Fig. 3). The S concentrations are highest in basaltic MIs with a mean of 1010±380 ppm, decreasing with increasing SiO_2 to 650±300 ppm in intermediate to 80±60 ppm in silicic MIs (Fig. 3a). Most variability is seen basaltic MIs, where S is lower (~300-1300 ppm) in primitive high-MgO (> 10 wt.%) basalts and increases with decreasing MgO toward peak S contents (~1000-2630 ppm) at about 5 wt.% MgO (Fig. 3b). At the low-MgO side of this inflexion point, S contents steadily decrease toward intermediate and silicic rocks, which have 0-240 ppm S. Highest MI S contents occur in the SIVZ eruptions of Hekla (1910 CE), Katla (Eldgjá 934 CE) and Surtsey (1963-67 CE) (Fig. 3a). Subaerially erupted tephra matrix glasses have generally low S concentrations (from 0 to few 100s of ppm) relative to MIs from the same eruption.

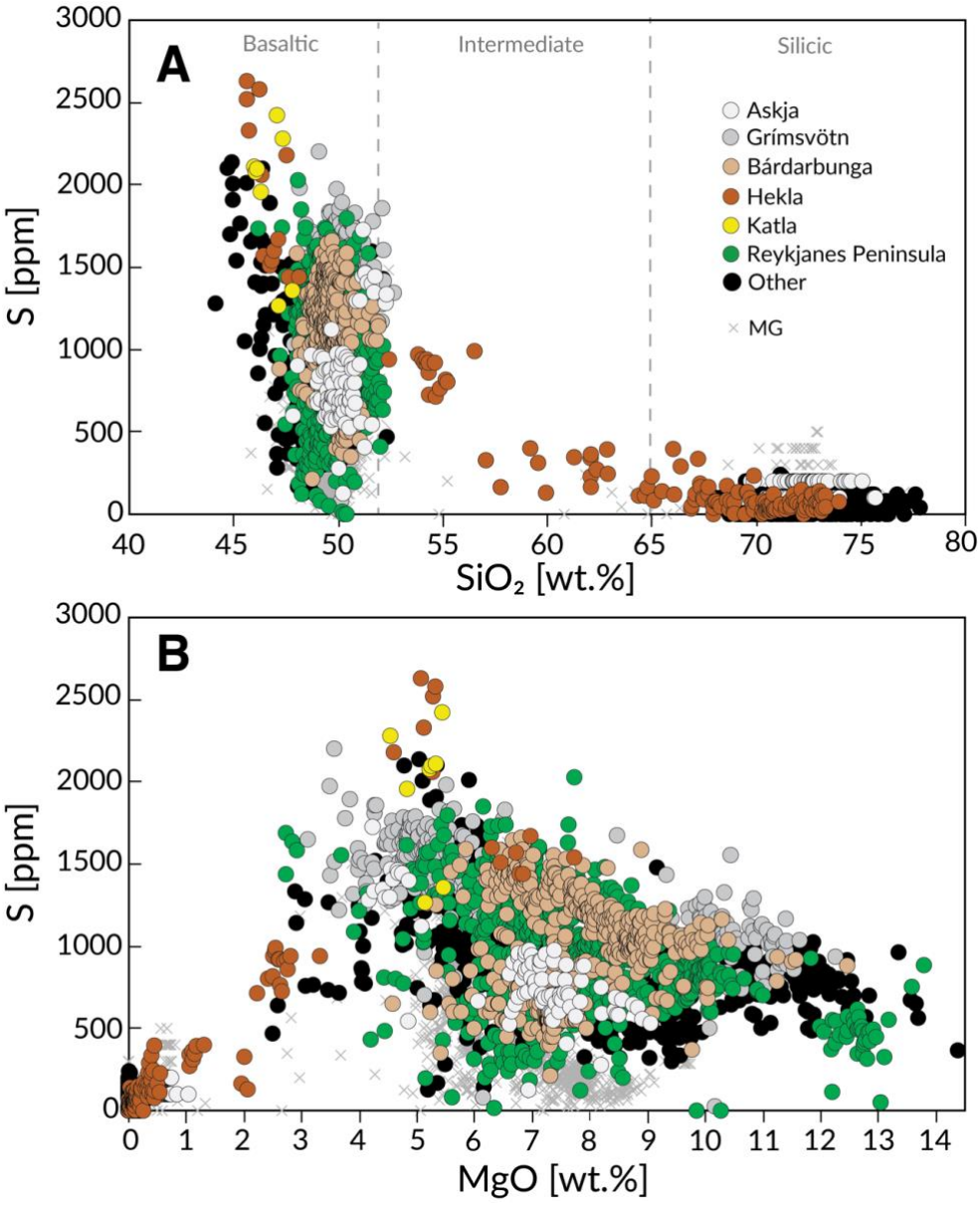

Figure 3. Compositional controls on sulfur contents of Icelandic melt inclusions. S vs. (a) SiO_2, and (b) MgO.

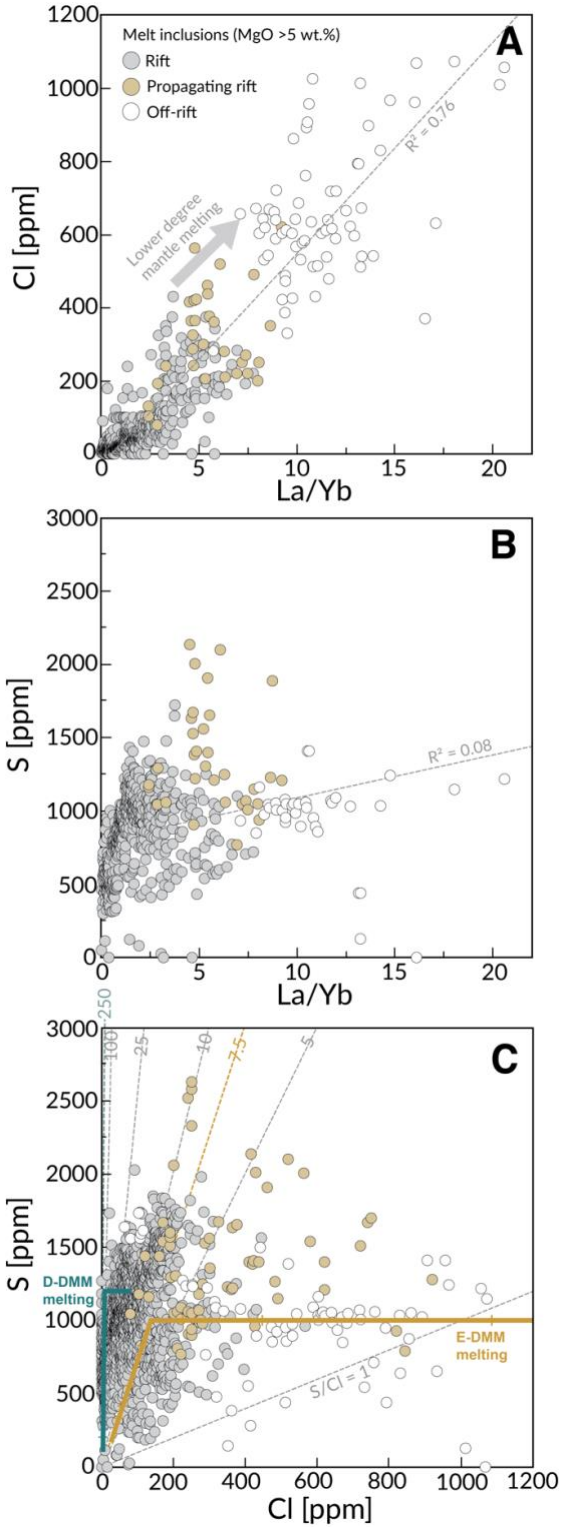

Figure 4. Effect of mantle melting and source heterogeneity on (a) Cl vs La/Yb, (b) S vs. La/Yb, and (c) S vs Cl systematics. Good correlation of Cl, and poor correlation of S with La/Yb indicates decoupling of S from Cl during the mantle melting process. The teal and amber model curves in panel (c) track fractional mantle melting of depleted (D-DMM) and enriched (E-DMM; amber) endmembers (Shimizu et al., 2016) of the depleted mantle source of mid-ocean ridge basalts (DMM) under initially sulfide saturated conditions (see Fig. 5). The resulting fractionation of the S/Cl ratio suggests that source heterogeneity and variable degree of melting could explain the bulk of the observed MI S/Cl variability. Model parameters are given in Table S8.

5 Discussion

5.1 Controls on sulfur contents of Icelandic magmas

5.1.1 Mantle source, partial melting and regional variability

Sulfur contents of primary basaltic melts are essentially controlled by the S content and the extent of melting of their mantle source. A number of studies have shown that the mantle beneath Iceland is heterogeneous with respect to the volatile origin (and probably, volatile concentrations) on a regional scale (e.g., Kurz et al., 1985; Poreda et al.; 1986, Hilton et al. 2000; Nichols et al., 2002; Füri et al., 2010; Halldórsson et al., 2016a, 2016b; Harðardóttir et al., 2018; Miller et al., 2019; Matthews et al., 2021; Marshall et al., 2022; Ranta et al., 2022). Given this, and that the degree of mantle melting is largely controlled by the tectonic setting and lithospheric thickness—melting degree being higher near the rift zones, and lower in the off-rift zones (Harðardóttir et al., 2022)—regional variations are expected to be expressed in MI volatile concentrations. For example, 2% partial melting of a hypothetical mantle component A with 200 ppm H_2O (assumed to be perfectly incompatible) will yield a primary basaltic melt with 1 wt.% H_2O, whereas 20% partial melting produces a melt with 0.1 wt.% H_2O—a factor of 10 less (assuming accumulated fractional melting). On the other hand, if mantle component B has 1000 ppm H_2O (i.e., 5x mantle component A), any equal degrees of melting of A and B will lead to a 5x difference in the H_2O contents of their respective primary melts. These differences are well within the suggested variability in both the degree of melting across different volcanic regions of Iceland (e.g. Koornneef et al., 2012) and the range of volatile concentrations inferred for the enriched and depleted mantle sources of mid-ocean ridge basalts (MORBs; Shimizu et al., 2016).

Such regional controls appear to influence H_2O and Cl, and to a lesser extent F concentrations of Icelandic basalts. Highest H_2O (up to 1.6 wt.% at Ljósufjöll and 1.5% in Surtsey), Cl (up to 2410 ppm at Fimmvörðuháls, 1880 ppm in Snæfellsjökull, 1260 ppm at Ljósufjöll) and F (2850 ppm, Ljósufjöll) concentrations are all seen in MIs of off-rift basalts in the SIVZ and SNVZ, whereas rift basalts (NRZ, ERZ, WRZ, RP) typically have lower concentrations of H_2O (< 0.8 wt.%), Cl (< 500 ppm) and F (< 800 ppm) (Figs. S2 and 4). The Cl concentrations in basaltic MIs correlate with La/Yb (Fig. 4a, $R^2 = 0.76$). Higher La/Yb ratios in Iceland indicate decreasing melt degree, deeper melting and higher proportion of melts derived from an enriched mantle component (e.g., Schilling 1973; Koornneef et al., 2012; Harðardóttir et al., 2022).

However, regional systematics do not appear to govern magmatic S contents, which are similar at both rift and off-rift regions at similar MgO or SiO_2 contents (Fig. 3) and do not correlate with La/Yb (Fig. 4b; $R^2 = 0.08$). To investigate which additional process controls melt S concentrations, we inspect the MI S/Cl ratio, which should stay approximately constant during partial melting and fractional crystallization due to the similar incompatibility of both elements in relevant silicate minerals (Baker et al., 2023). Off-rift MIs have low S/Cl ratios between 0.5 and 5, lower than either the depleted (S/Cl ≈ 250) or enriched (S/Cl ≈ 7.5) mantle endmembers inferred for the depleted MORB source mantle (D-DMM and E-DMM, respectively; Shimizu et al., 2016; Fig. 4c). By contrast, highly depleted MIs in rift basalts (products of high-degree melting) have high S/Cl ratios (>100) approaching the S/Cl signature of D-DMM (Fig. 4c). The decoupling of S and Cl systematics suggests that S concentrations in primary melts are buffered by sulfide saturation during mantle melting, in accord with previous work (Momme et al., 2003; Ding and Dasgupta 2018).

We modelled the effect of partial mantle melting on S and Cl concentrations and S/Cl ratios of primary melts under the assumption that sulfur in the melting region is hosted exclusively in sulfides (Ding & Dasgupta, 2018). Two mantle endmember compositions were used to simulate depleted and enriched mantle components under Iceland (e.g., Gurenko & Chaussidon, 1995; Hanan et al.,

2000; Shorttle et al., 2011; Koorneef et al., 2012) which were assumed to have S, Cl, La and Yb concentrations of the D-DMM and E-DMM (Workman and Hart 2005, Shimizu et al., 2016; Figs. 4c and 5). The melting model of Lee et al. (2012) implemented in the open source Python3 tool PySulfSat (Wieser & Gleeson, 2023) was used for the calculations. Full model parameters are given in Table S8.

Similar to the results of Ding and Dasgupta (2018), our modelling indicates that sulfide saturation persists under low- to moderate-degree mantle melting ($F < 0.8–0.16$). Thus, off-rift melting (typically $F < 0.1$, Harðardóttir et al., 2022) likely occurs under sulfide-saturated conditions, whereas higher melt degrees under rift zones (typically $F > 0.16$, Harðardóttir et al., 2022) are generally sufficient to completely exhaust sulfides from the mantle source (Fig. 5a–b). During sulfide-saturated melting (off-rift), the S concentrations of accumulated fractional melts are approximately constant (Fig. 5a). With increasing melt-degree, Cl concentrations gradually decrease, causing the S/Cl ratio to increase until sulfides originally present in the mantle source are exhausted completely. At this point, the S/Cl ratio of primitive melts approaches that of the mantle source and remains approximately constant during further melting (Fig. 5b). Thus, the variable S/Cl ratios of high-MgO MIs reflect both the degree of melting and the S and Cl composition of the source mantle.

The S/Cl variability of Icelandic MIs can be explained by melting of D-DMM and E-DMM with S and Cl concentrations of 100 and 0.4 ppm (D-DMM) and 165 and 22 ppm (E-DMM), respectively (Shimizu et al., 2016). These mantle concentrations are within previously estimated peridotite S concentrations of 100–150 ppm for Iceland (Ding and Dasgupta 2018) and S of 50-200 ppm and Cl of 3-15 ppm for the mantle source(s) of the Holuhraun 2014-15 eruption (Bali et al., 2018). For the used model parameters, the lowest S/Cl ratios are produced by low-degree melting (e.g., S/Cl = 1 at F = 2%) of the E-DMM. The majority of S/Cl and La/Yb ratios of the most enriched the off-rift lavas can be matched by 2–7% melting of E-DMM (Fig. 5c). By contrast, high S/Cl of up to 250 is produced by high-degree melting ($F > 10\%$) of the D-DMM component at sulfide-saturated conditions, which aligns well with highly depleted melt inclusions found in rift lavas (e.g., Bali et al., 2018). Melt inclusions that fall below the partial melting curves in the S/Cl vs. La/Yb space could be explained by binary mixing of enriched and depleted melts (mixing curve for 2% E-DMM melt and 20% D-DMM is shown for illustrative purposes in Fig. 5c).

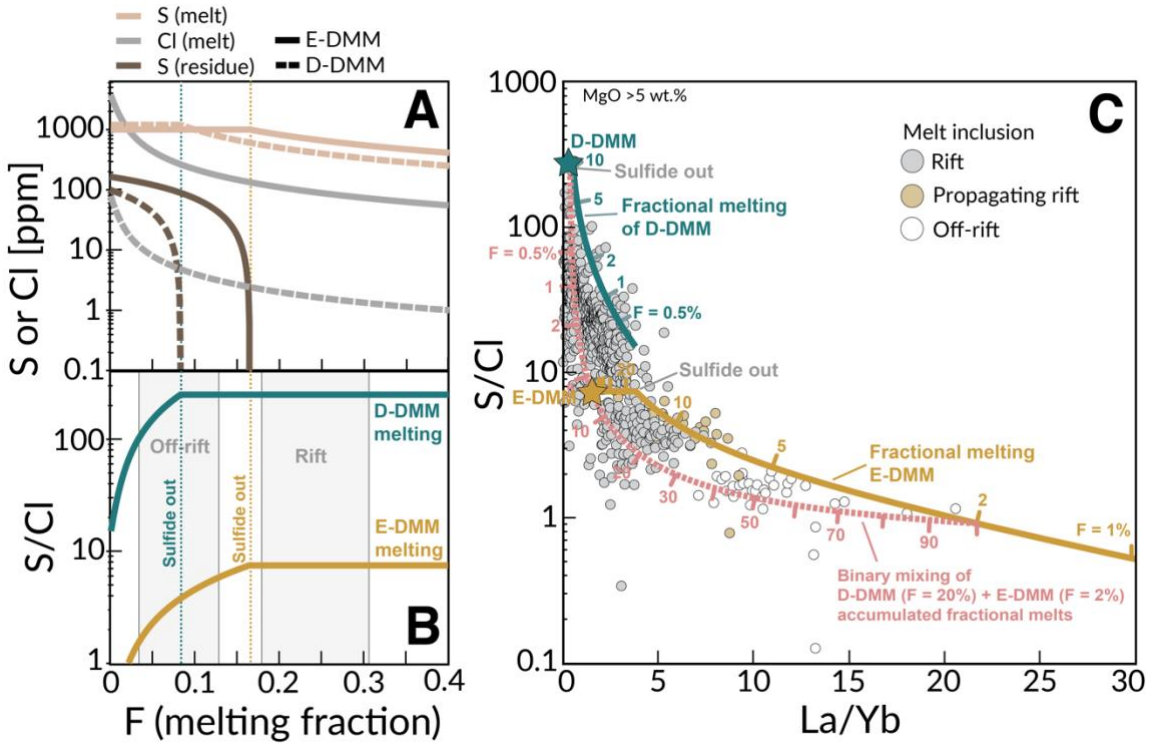

Figure 5. Effect of sulfide-saturated partial mantle melting on **(a)** S and Cl of aggregate fractional melts vs. F (melt fraction), **(b)** S/Cl vs. melting fraction (F), and **(c)** S/Cl vs. La/Yb. Melting model of Lee et al. (2012) was implemented in PySulfSat (Wieser & Gleeson, 2023) to emulate fractional melting of a depleted (D-DMM) and mildly enriched (E-DMM) source lithology previously suggested for MORBs (Shimizu et al., 2016). The teal and amber model curves in panels (b) and (c) track the melt concentrations of accumulated fractional melts. The red curve in (c) shows binary mixing of a 2% E-DMM melt and a 20% D-DMM melt. The good match between observed and modelled S/Cl vs La/Yb trends suggests that MI S/Cl ratios reflect various degrees of melting of the D-DMM and E-DMM mantle components and subsequent melt mixing. Model parameters are reported in Table S8. Only melt inclusions with MgO > 5 wt.% are plotted in panel (c) to minimize the effect of sulfide melt immiscibility during crustal magma evolution.

5.1.2 Effects of crustal magma evolution on S and SCSS

Fractional crystallization during crustal magma evolution leads to increasing concentrations of dissolved volatiles, which tend to behave as incompatible elements in silicate melts, but only until volatile-bearing fluid or solid phases are saturated (e.g., Shima & Naldrett, 1975; O'Neill & Mavrogenes, 2002; Hughes et al., 2023). The effects of S degassing and sulfide melt immiscibility on pre-eruptive S concentrations of Icelandic magmas are discussed below.

With respect to vapor saturation, S has an intermediate solubility in basaltic melts, being more soluble than CO_2 but less soluble than H_2O at a given pressure (Wallace & Edmonds, 2011). Basaltic melts in Iceland, which are H_2O-poor (< 1.5 wt.%, Fig S2a) and have an oxygen fugacity close to the fayalite-magnetite-quartz buffer FMQ (Óskarsson et al., 1993; Novella et al., 2020; van der Meer et al., 2021) should remain undersaturated with respect to a sulfur-bearing vapor phase at typical magmatic storage pressures (~1-10 kbar; Fig. 6; Neave et al., 2019; Baxter et al., 2023; Ding et al., 2023). Indeed, modelling of degassing of Icelandic basalts suggests that bulk of the dissolved sulfur in Icelandic basaltic melts is degassed at very low pressures of < 0.2 kbar (Fig. 6; Sigmundsson et al., 2019; Ranta et al., 2023). From a volcano monitoring perspective, it is important to note that more H_2O-rich basaltic andesite melts (such as the Hekla 2000 eruption) can start degassing sulfur

at greater pressures of ~0.8 kbar (Fig. 6). Thus, the melt inclusion S record, at least for basaltic MIs, should reflect near-undegassed melt contents at the time of entrapment.

However, formation of an immiscible sulfide liquid at the sulfide solubility limit has for long been recognized as an important factor that buffers the S (and chalcophile element) budgets of both arc-related (Jenner et al., 2010; Lee et al.; 2012) and mid-ocean ridge basalts (MORBs) (Mathez, 1976), as well as many ocean plateau and hotspot lavas (Labidi et al., 2015; Reekie et al., 2019; Wieser et al., 2020) including Iceland (Momme et al., 2003; Ranta et al., 2022). In Icelandic melts, a smoking gun evidence for sulfide saturation is provided by decreasing concentrations of Cu—which is incompatible in silicate minerals but strongly compatible in the forming monosulfide liquid (Kiseeva & Wood, 2015)—with decreasing MgO below approximately 6 wt.% MgO in subglacial pillow rim glasses (Ranta et al., 2022). Whether higher-MgO melts reach sulfide saturation (hereafter measured as sulfur concentration at sulfide saturation, SCSS) is not entirely clear from previous data (Ranta et al., 2022).

We used the SCSS model of Smythe et al. (2017), implemented in PySulfSat (Wieser & Gleeson 2003), to calculate the SCSS for all MIs in IMIC (Fig. 7). The SCSS depends on melt composition (in particular, SCSS increases with increasing FeO), pressure (higher P decreases SCSS), temperature (higher T increases SCSS), oxygen fugacity (S^{2-} oxidizes to S^{6+}, which has a higher solubility, above approximately FMQ+0.5; Jugo et al., 2010) and sulfide composition (Shima & Naldrett, 1975; O'Neill & Mavrogenes, 2002; Kiseeva & Wood, 2015; Smythe et al., 2017; Nash et al., 2019; O'Neill, 2021; Ding et al., 2023; Hughes et al., 2023). The choice of SCSS model does not radically affect the following discussion: for example, the O'Neill (2021) and Li and Zhang (2022) models generally yield similar-shaped SCSS curves at slightly higher and lower SCSS (Fig. 7a-b), respectively, but within the estimated 1σ uncertainty (~300 ppm) of the Smythe et al. (2017) model. For the modelling parameters, we used reported MI major element compositions, Fe^{3+}/Fe_{tot} = 0.1, P = 2 kbar and T calculated with the major element composition-based liquid thermometer of Putirka (2008; Eq. 14).

The modelling highlights the dominant effects of FeO and T on the modelled SCSS. Decreasing temperature lowers the SCSS, but also causes crystal fractionation and decreasing MgO (Fig. 7a). The opposing effects of FeO and T on the SCSS lead to zig-zagging liquid lines of descent in a FeO vs. SCSS diagram for a typical tholeiitic fractionation path (Fig 7b). At early stages of tholeiitic basaltic melt evolution characteristic for Icelandic rift zones, fractional crystallization of olivine ± clinopyroxene ± plagioclase causes melt FeO to increase with *decreasing T* and decreasing MgO. Following the onset of magnetite crystallization at ~5 wt.% MgO, both FeO and T decrease causing SCSS to drop (Fig. 7a–b).

Importantly, this leads to a local maximum in both calculated SCSS and observed S concentrations (1200–2600 ppm) seen in evolved basaltic melt inclusions at about 5 wt.% MgO, coinciding with maximum melt FeO contents (> 14 wt.%, Fig. S3a). Subsequent melt evolution leads to systematically decreasing S and ΔS due to decreasing SCSS, which rapidly decreases as FeO decreases (O'Neill & Mavrogenes 2002; Smythe et al., 2017; Fig. 7b). These effects explain why moderate S concentrations are observed in basaltic andesites, and lowest S are systematically found in dacites and rhyolites (Figs. 3a, 8a).

That the calculated SCSS of the MIs recreates some of the main features traced by the upper limit of measured MI S concentrations at a given MgO suggests that at least the maximum melt S content is limited by SCSS at all MgO contents. However, in general, most MIs with MgO > 6 wt.% have S concentrations below SCSS (Fig. 7d), compatible with similar MgO threshold for sulfide saturation suggested previously for Icelandic melts (Ranta et al., 2022). The range of possible fractional crystallization paths likely allows both S saturated and undersaturated high-MgO melts. Melts below 4 wt.% MgO appear to virtually all be above or close to SCSS (Fig. 7d).

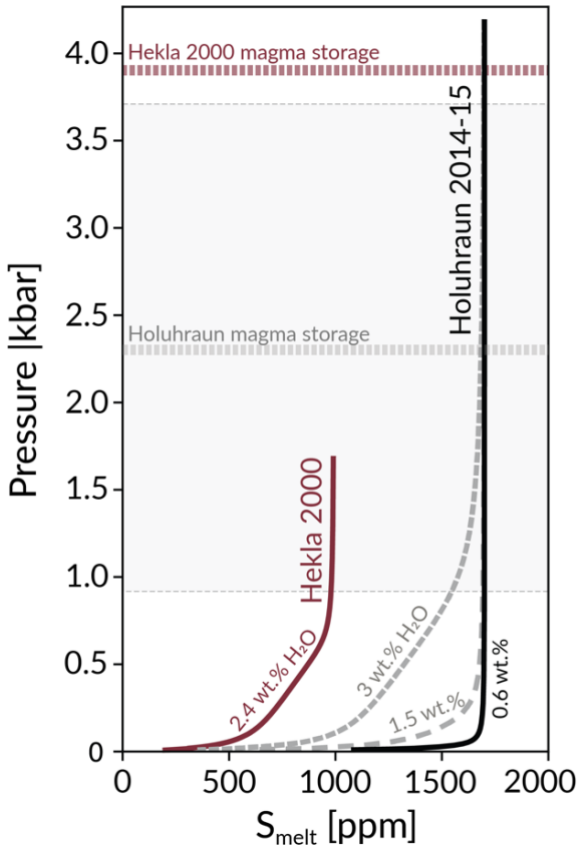

Figure 6. Sulfur degassing. Modelled closed-system sulfur degassing paths are shown for the basaltic Holuhraun 2014-15 eruption (black solid line), which was a typical rift zone fissure eruption, and the basaltic andesite Hekla 2000 eruption (red solid line), a common composition for the Hekla volcano. Assuming pre-eruptive melt H_2O and S contents inferred from melt inclusions, the model predicts insignificant S degassing at the estimated magma storage pressures for both Holuhraun (2.3±1.4 kbar; Halldórsson et al., 2018) and Hekla 2000 (3.9 kbar, calculated from an estimated magma storage depth of >14 km and mean crustal density of 2860 kg/m^3; Höskuldsson et al., 2007). Addition of water to the Holuhraun melt (two dashed grey curves) allows the onset of S degassing at greater pressures (cf. Ding et al., 2023). However, water contents above 1.5 wt.%, required for significant degassing to occur above the approximate lower limit of 1 kbar of basaltic magma reservoirs in Iceland (Neave et al., 2017b), are not seen in Icelandic basaltic melt inclusions (Fig. S2a). This implies that S concentrations of basaltic MIs in Iceland reflect virtually undegassed melts. Degassing paths were calculated with the open source COHS-degassing model Sulfur_X (Ding et al., 2023) using the COH model of Newman and Lowenstern (2002), S speciation model of O'Neill and Mavrogenes (2022) and oxygen fugacity buffered at ΔFMQ = 0. Pre-eruptive volatile concentrations were chosen as 0.61 wt.% H_2O, 1700 ppm CO_2 and 1700 ppm S for Holuhraun (Bali et al., 2018) and 2.4 wt.% H_2O (Table S2), 500 ppm CO_2 (arbitrarily chosen due to lack of data) and 990 ppm S for Hekla 2000 (Table S2). Major element compositions used were averages of matrix glasses (Table S2).

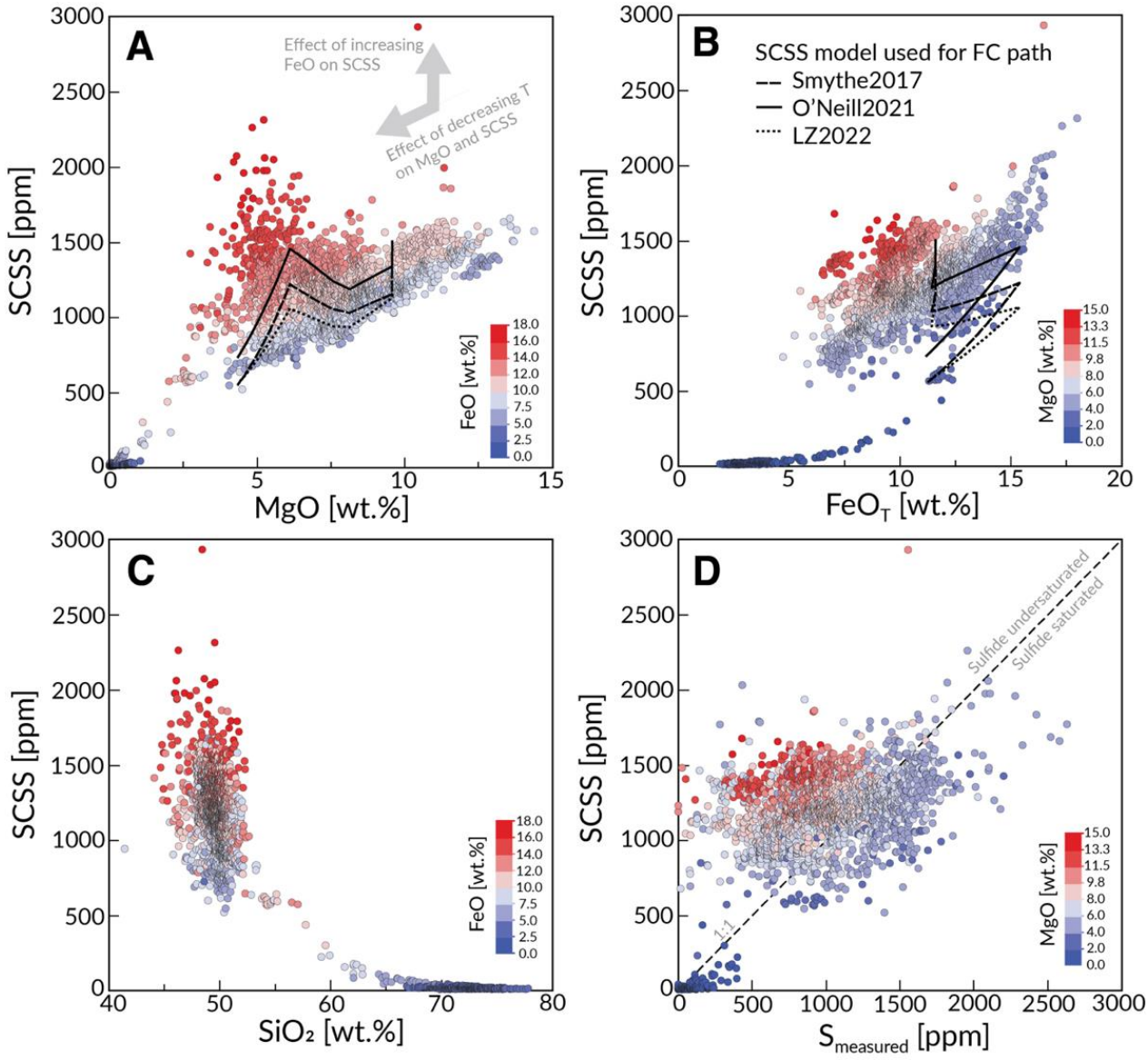

Figure 7. Modelled SCSS (sulfur concentration at sulfide saturation) of Icelandic melts vs. **(a)** MgO, **(b)** FeO_T, **(c)** SiO_2 and **(d)** measured S concentrations. Circles, colored after the FeO (a and c) or MgO (b and d) content, show SCSS for raw melt inclusion data, calculated using the Smythe et al., (2017) model (see text for model parameters). An example SCSS along a fractional crystallization path is shown for a PEP-corrected melt inclusion composition (NAL-356; Ranta et al., 2022), produced by isobaric (3 kbar) closed-system fractional crystallization in the Petrolog3 software (Danyushevsky & Plechov, 2011) Dashed, solid and dotted lines show the SCSS calculated after Smythe et al., (2017), O'Neill (2021) and Li and Zhang (2022), respectively. The fractional crystallization path illustrates the main features seen in empirical data, but reaches magnetite saturation at slightly higher MgO. Negative effect of P on SCSS means that the SCSS for MIs trapped at greater depths than the modeled 2 kbar may be over-estimated, and vice versa. All SCSS models were implemented in the open source PySulfSat code (Wieser & Gleeson, 2023).

5.2 Magmatic volatile phases and excess degassing

An inherent assumption of the petrological method is that volatiles that degas during an eruption are solely derived from the volume of the erupted lava. This assumption does not account for volatiles that may coexist with magmas in a separate magmatic volatile phase (MVP), which may be an

accumulative product of deep degassing and/or fluids derived from a larger volume of intrusive magma that has reached volatile saturation in the magma storage region (Shinohara, 2008; Hartley et al., 2014; Edmonds & Wood, 2018; Ranta et al., 2021). Thus, the petrological estimate (only accounting for the dissolved volatiles) may underestimate the total volatile emissions (dissolved volatiles + MVP). One of the main factors controlling the volatile saturation state of a magma, and thereby, the development of a MVP, is the pre-eruptive magma storage pressure (Fig. 6).

Underestimation of S emissions by the petrological method has been frequently observed at arc volcanoes, something known as the 'excess degassing problem' (e.g. Andres et al., 1991; Gerlach and McGee 1994; Sharma et al., 2004; Shinohara, 2008; Su et al., 2016). To account for existence of a separated MVP, a modified petrological method was proposed by Scaillet and Pichavant (2003) and Scaillet et al. (2003), where 1-5 wt.% of free gas phase at depth was added to the petrological estimate. However, such correction is not needed for basaltic eruptions in Iceland, as the amount of MVP in these magma reservoirs is likely to be significantly lower due to their low H_2O contents (0.05-1.5 wt.%; Nichols et al., 2002; Fig. S2a) relative to arc magmas (> 2 wt.%; Plank et al., 2013). At typical Icelandic magma reservoir pressures of 1–10 kbar (Neave et al., 2017b; Baxter et al., 2023), virtually all S (and H_2O, Cl and F) in the relatively dry basaltic melts remains dissolved in the melt at the observed concentration range (e.g., Wallace & Edmonds 2011; Fig. 6). Thus, the petrological method is suitable for calculating S emissions of Icelandic volcanoes.

It is likely that relatively long-lived silicic magma reservoirs in Iceland develop MVPs (Ranta et al., 2021), which could provide significant sources of excess degassing that are not accounted for by the petrological method. However, as no silicic eruptions have occurred during recent history in Iceland, S degassing (and that of other volatiles) accompanying silicic volcanism in Iceland remains poorly constrained. An interesting observation in that regard is that matrix glasses in the silicic Askja 1875 CE eruption have higher S content than the corresponding melt inclusions (Fig. 3a), which could indicate an enrichment in S caused by influx of deeper-derived gases from mafic intrusions or recharge melts (Helgason et al., 1992; Watkins et al., 2017). An important task for future research is to better understand both volcanic S and halogen (particularly F) pollution hazards of silicic eruptions in Iceland.

5.3 Empirical verification of the petrological estimate of SO_2 emissions

5.3.1 Effusive eruptions

A critical accuracy test of the petrological method is to compare estimated SO_2 emissions with direct volcanic gas measurements. The best available test cases in Iceland are the recent Holuhraun 2014-15 (Bali et al., 2018; Pfeffer et al., 2018) and Fagradalsfjall 2021 (Pedersen et al., 2022; Halldórsson et al., 2022, Barsotti et al., 2023; Pfeffer et al., *submitted*) basaltic fissure eruptions. Both eruptions lasted about 6 months and were closely monitored using ground-based measurements for their lava effusion rates, lava volumes and gas fluxes. The average lava effusion rate (90 m^3/s) and total lava volume (1.44 km^3 incl. vesicles) of Holuhraun (Pedersen et al., 2017) were approximately 10-fold compared to the 9.5 m^3/s and 0.15 km^3, respectively, measured for Fagradalsfjall (Pedersen et al., 2022). In both cases, the total SO_2 emissions derived from petrological estimates and gas measurements match remarkably well; the petrological estimate of 10.5 Mt SO_2 for Holuhraun (Bali et al., 2018) compares well with the 9.6 (6.7-14.3) Mt SO_2 (Pfeffer et al., 2018) derived from direct plume measurements by differential optical absorption spectroscopy (DOAS). Similarly, for Fagradalsfjall, the petrological method yields 0.9 Mt SO_2, matching with 0.97±0.54 Mt SO_2 determined by DOAS (Barsotti et al., 2023; Pfeffer et al., *submitted*).

Petrological estimates of SO_2 have further been shown to agree reasonably well with satellite-based measurements using the Total Ozone Mapping Instrument (TOMS; Sharma et al., 2004) for the Krafla 1984 (0.64±0.19 vs. 0.4+0.04–0.15 Mt) and Hekla 2000 (0.48±0.14 vs. 0.10±0.05 Mt)

eruptions (Sharma et al., 2004). By contrast, similar comparisons at arc volcanoes sometimes show orders of magnitude higher TOMS SO_2 emissions relative to petrological estimates (Sharma et al., 2004). The close match between direct SO_2 measurements with the petrological method for hitherto observed Icelandic fissure eruptions provides an empirical validation of the petrological method as an accurate means to estimate volcanic SO_2 emissions of basaltic fissure eruptions in Iceland.

5.3.2 Explosive eruptions

Comparable direct and petrological SO_2 emission estimates are available for two Icelandic explosive eruptions (i.e., where eruption products were dominated by high-altitude, ash-containing plumes): Hekla 1980 (Sharma et al., 2004) and Grímsvötn 2011 (Sigmarsson et al., 2013). The two methods match reasonably well for the Hekla 1980 eruption (0.36±0.12 Mt SO_2 vs. 0.50±0.10 Mt SO_2 via TOMS). However, the estimated S emissions for the Grímsvötn 2011 eruption are about five times lower using the NASA satellite-borne Ozone Monitoring Instrument (OMI) (0.2 Mt S, or c. 0.3 Mt including estimated S scavenging on tephra surfaces; Olsson et al., 2013) relative to the petrological method (1.47±0.36 Mt, Sigmarsson et al., 2013; Haddadi et al., 2017).

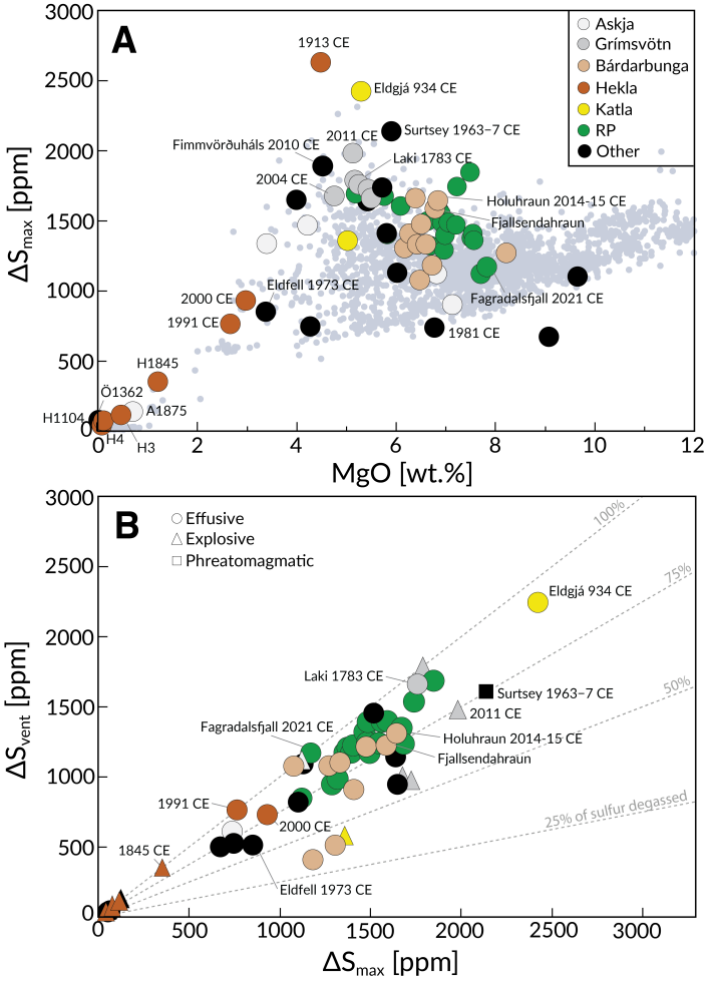

Figure 8: Petrological S emission estimates (a) ΔS_{max} vs. MgO. Pale blue dots show SCSS for raw MI data calculated after Smythe et al. (2017) in PySulfSat (Weiser & Gleeson, 2023). (b) Total sulfur emission potential ΔS_{max} compared to vent sulfur emissions (ΔS_{vent}). There is no obvious correlation between eruption type (explosive, effusive, phreatomagmatic) and ΔS. Plotted major

element compositions of eruptions in Figs. 8a and 9a are based on average matrix glass compositions (Table S2).

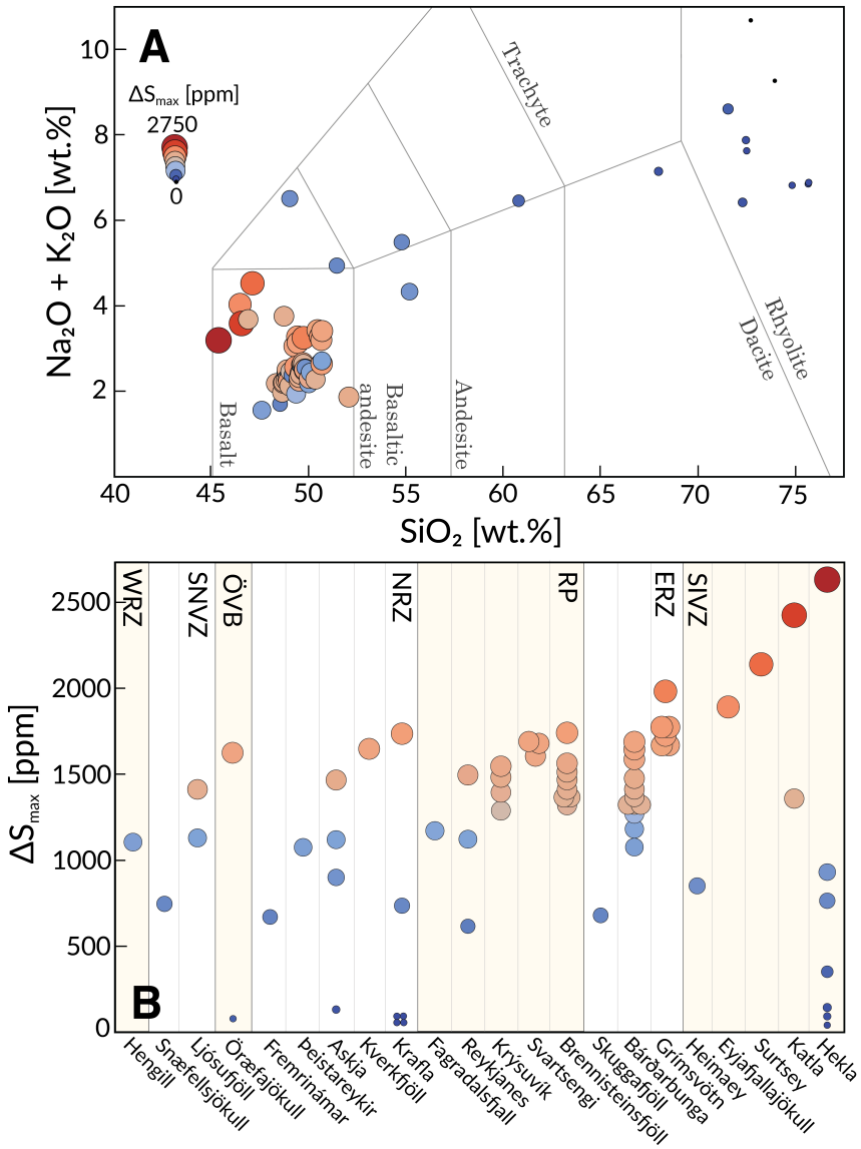

Figure 9. Summary figure of the sulfur emission potentials (ΔS_{max}) of Icelandic volcanoes. (a) TAS diagram. Circles represent individual eruptions and are shaded from blue to red, and increase in size, with increasing ΔS_{max}. (b) ΔS_{max} sorted by volcano. Volcanoes are grouped by volcanic zone and increasing ΔS_{max}.

Table 2: Sulfur emission potentials

Eruption*	Volcano	Zone	Composition	V (km^3)**	ΔS_{vent}	ΔS_{max}	S release (Tg)	SiO_2[a]	MgO	Na_2O+K_2O[b]
Holuhraun (old)	Bár	ERZ	Basaltic			1077		49.6	6.5	2.6
Veiðivötn 1477 CE	Bár	ERZ	Basaltic	*2.2*	1103	1332	7.94	49.6	6.4	2.6
Ljósufjöll	Bár	ERZ	Basaltic		1079	1271		49.4	8.2	1.9
Þjórsárdalshraun	Bár	ERZ	Basaltic		1216	1476		48.9	6.5	2.5
Fontur[c]	Bár	ERZ	Basaltic		513	1306		49.7	6.2	2.6
Brandur[c]	Bár	ERZ	Basaltic		410	1183		50.1	6.7	2.4
Saxi[c]	Bár	ERZ	Basaltic		910	1408		49.6	6.3	2.4
Holuhraun 2014-15 CE	Bár	ERZ	Basaltic	1.44	1311	1644	6.42	49.8	6.8	2.5
Fjallsendahraun	Bár	ERZ	Basaltic	4	1225	1587	17.2	49.7	6.8	2.7
Þjórsárhraun	Bár	ERZ	Basaltic	25		1661	113			
Skuggafjöll	Bár	ERZ	Basaltic			681				
2004 CE	Grí	ERZ	Basaltic	*0.021*	1006	1677	0.095	50.5	4.8	3.4
Laki 1783 CE	Grí	ERZ	Basaltic	15.1	1662	1759	72.0	49.4	5.2	3.3
1823 CE	Grí	ERZ	Basaltic		1253	1660		50.7	5.5	3.2
1873 CE	Grí	ERZ	Basaltic		1789	1789		50.6	5.2	3.3
2011 CE	Grí	ERZ	Basaltic	*0.2-0.3*	1480	1982	1.34	49.8	5.1	3.2
Saksunarvatn Middle	Grí	ERZ	Basaltic			1725		49.5	5.4	3.1
1875 CE	Ask	NRZ	Silicic	0.32	-161	139	0.121	72.3	0.7	6.4
Askja NE tuff	Ask	NRZ	Basaltic			902		49.8	7.1	2.5
Askja SW tuff	Ask	NRZ	Basaltic			1122		50.7	6.8	2.7
Nýjahraun	Ask	NRZ	Basaltic	0.345		1468	1.37	52.1	4.2	1.9
Heilagsdalsfjall	Fre	NRZ	Basaltic		501	673		48.6	9.1	1.7
Gæsarfjallarani	Kra	NRZ	Silicic	0.15		69	0.028			
Hlíðarfjall	Kra	NRZ	Silicic	0.14	53	53	0.020	75.7	0.1	6.9
Jörundur	Kra	NRZ	Silicic	0.15	63	63	0.025	74.9	0.1	6.8
Víti	Kra	NRZ	Silicic		48	48		75.7	0.1	6.9
Hverfjall	Kra	NRZ	Basaltic		1528	1737		50.7	5.7	2.6
1981 CE	Kra	NRZ	Basaltic		612	738		49.2	6.8	2.4
Kverkfjöll-subglacial	Kve	NRZ	Basaltic		947	1649		50.7	4.0	3.4
Borgarhraun	Þei	NRZ	Basaltic			1077				
1362 CE	Ör	ÖVZ	Silicic	1.2	77	240	0.780	71.5	0.0	8.6
Fagradalsfjall 2021 CE	Fag	RP	Basaltic	0.15	1171	1171	0.476	50.0	7.8	2.2
Húsfellsbrúni	Bre	RP	Basaltic	0.2	1392	1485	0.805	48.9	7.0	2.3
Hvammahraun	Bre	RP	Basaltic	0.72	1684	1850	3.61	49.0	7.5	2.1
Kistuhraun	Bre	RP	Basaltic	0.08	1321	1467	0.318	48.8	7.2	2.2
mið-Húsfellsbruni	Bre	RP	Basaltic	0.05	1537	1740	0.236	49.0	7.2	2.2
Selvogshraun	Bre	RP	Basaltic	0.19	1225	1405	0.723	48.4	7.5	2.2
Svartihryggur	Bre	RP	Basaltic	0.0005	987	1319	0.002	48.9	6.7	2.3
Svínahraunsbrúni	Bre	RP	Basaltic	0.06	1393	1563	0.254	48.7	6.9	2.2
Tvíbollahraun	Bre	RP	Basaltic	0.37	1173	1357	1.36	48.7	7.6	2.0
Hrútafellshraun	Krý	RP	Basaltic	0.04	1241	1546	0.168	49.5	6.9	2.2
Kapelluhraun	Krý	RP	Basaltic	0.07	1173	1394	0.264	49.6	7.0	2.4
Mávahlíðarhraun	Krý	RP	Basaltic	0.02	947	1288	0.070	49.1	7.0	2.5
Ögmundarhraun	Krý	RP	Basaltic	0.13	1246	1482	0.522	49.5	6.9	2.3
Stapafell	Rey	RP	Basaltic		849	1122		49.0	7.7	2.4
Háleyjabunga	Rey	RP	Basaltic			617				
Stampahraun-4	Rey	RP	Basaltic	0.1	1171	1495	0.405	50.1	6.6	2.3
Arnarseturshraun	Sva	RP	Basaltic	0.55	1392	1604	2.39	49.2	6.1	2.6
Eldvarpahraun	Sva	RP	Basaltic	0.28	1350	1676	1.27	49.4	5.8	2.5
Illahraun	Sva	RP	Basaltic	0.05	1240	1689	0.229	48.8	5.2	2.5
Fimmvörðuháls 2010 CE	Eya	SIVZ	Basaltic	0.02		1890	0.102	46.2	4.5	4.0
Eldfell 1973 CE	Hei	SIVZ	Basaltic	*0.21*	997	1334	0.759	49.1	3.4	6.5
H4	Hek	SIVZ	Silicic	*2.5*	39	42	0.284	72.5	0.1	7.6
1104 CE	Hek	SIVZ	Silicic	*0.5*	74	74	0.101	72.5	0.1	7.9
H3	Hek	SIVZ	Silicic	*2.5*	115	115	0.780	68.0	0.5	7.1
1845 CE	Hek	SIVZ	Intermediate	*0.06*	352	352	0.057	60.8	1.2	6.5
1991 CE	Hek	SIVZ	Intermediate	*0.006*	765	765	0.012	54.8	2.7	5.5
2000 CE	Hek	SIVZ	Intermediate	*0.002*	731	931	0.005	55.2	3.0	4.3
1913 CE	Hek	SIVZ	Basaltic	0.05		2630	0.356	45.4	4.5	3.2
Eldgjá 934 CE	Kat	SIVZ	Basaltic	20	2245	2423	131	46.6	5.3	3.6
1357 CE	Kat	SIVZ	Basaltic	*0.1*	582	1358	0.368	46.9	5.0	3.7
1963-7 CE	Sur	SIVZ	Basaltic	1.1	1610	2138	6.37	47.1	5.9	4.5
Berserkjahraun	Ljó	SNVZ	Basaltic		1457	1520		48.8	5.8	3.7
Grábrókarhraun	Ljó	SNVZ	Basaltic		1093	1129		48.9	6.0	2.4
Ör1	Ör	SNVZ	Basaltic		1348	1499		46.6	5.2	3.7
Ör3	Ör	SNVZ	Basaltic		1238	1734		49.3	5.4	3.0
Djúpalónsvík	Snæ	SNVZ	Basaltic		526	746		51.5	4.3	4.9
Miðfell	Hen	WRZ	Basaltic		820	1102		47.6	9.7	1.5

[a] SiO_2, MgO, Na_2O+K_2O average value of matrix glass data.

[b] Mean MI S concentration, instead of maximum, used for calculating ΔS_{vent} and ΔS_{max} for silicic and intermediate eruptions

[c] Likely source craters of the ~8.6 ka Þjórsárhraun lava (Caracciolo et al., 2020)

*Data references for each eruption are shown in the electronic version of Table 2.

**Published volume estimates (Table S2). Values in italics indicate DRE values recalculated from tephra volume (Table S2)

5.4 Sulfur emissions of Icelandic eruptions

The sulfur emission potentials (ΔS_{max}, ΔS_{vent}) for 68 Icelandic eruptions, calculated with the petrological method, are summarized in Table 2 and Figs. 8-9. An extensive summary including calculation details, mean major element compositions and petrological estimates for the other volatiles is available in Table S2. In the discussion and the figures, we opt to use ΔS_{max}, which includes both vent degassing as well as degassing from the cooling lava field, and has been empirically shown to be close to total S emissions for Icelandic eruptions (Bali et al., 2018; Pfeffer et al., submitted)

5.4.1 Largest S emitters in Iceland

The largest pre-eruptive sulfur concentrations in Iceland (ΔS_{max} > 1200 ppm) are systematically found in evolved basalts (MgO between 4 and 8 wt.%; Fig. 8a) irrespective of volcanic zone (Fig. 9b). This is also the most common compositional range of Icelandic eruptions (Figs. 2a, 8a), including the most frequently erupting Holocene volcanoes Grímsvötn, Bárðarbunga and Katla and the largest Holocene eruptions by volume (Þjórsárhraun, Eldgjá 934 CE and Laki 1783 CE; Table 2). Basaltic eruptions at the higher end of this range (6-8 wt.% MgO), characterizing, e.g., Bárðarbunga and RP eruptions, have somewhat lower ΔS_{max} relative to the more evolved (4–6 wt.% MgO) eruptions typical of Katla and Grímsvötn (Fig. 8a).

Exceptionally high sulfur emission potentials (ΔS_{max} > 1800 ppm) are seen in five eruptions, all within a narrow range in MgO between 4.5 and 6 wt.% (Fig. 8a). This coincides with and even exceeds the apparent sulfide solubility peak in Icelandic melts (Fig. 7a; Ranta et al., 2022). Four of these eruptions, Eldgjá 934 CE, Hekla 1913 CE, Surtsey 1963-67 CE and Fimmvörðuháls 2010 CE, are located in the SIVZ and have a mildly alkaline composition (SiO_2 < 48 wt.%, TAS > 3 wt.%; Fig. 9a). Thus, up to 50% higher S emissions may be expected for basaltic eruptions in the SIVZ relative to average basaltic rift zone eruptions.

Compared to arc volcanoes (Oppenheimer et al., 2011), Icelandic eruptions tend to have higher ΔS (Fig. 10), and thus emit more sulfur per unit mass of erupted material. This is largely a function of the dominant eruption composition in Iceland (relatively evolved basalts) coinciding with a maximum in dissolved S contents. By contrast, although basaltic arc magmas can have even higher S contents (several thousands of ppm) due to their generally more oxidized nature (Wallace & Edmonds, 2011), basaltic arc eruptions are relatively uncommon. Notably, the total S emissions and emission rates of basaltic eruptions are principally controlled by the masses and mass fluxes of erupted material—which both vary by 3-5 orders of magnitude—rather than ΔS, which only varies by a factor of ~2-3x (Fig. 10).

The SO_2 hazard potential of volcanoes that consistently erupt lavas with similar compositions—like Bárðarbunga, Grímsvötn, Krýsuvík and Brennisteinsföll (Figs. 8a, 9b)—can be forecasted with less uncertainty based on our ΔS estimates, with uncertainty remaining due to factors including lava effusion rate and weather conditions. However, for volcanoes like Hekla that produce silicic, intermediate and evolved basaltic eruptions spanning the whole range of Icelandic S emission potentials, the pre-eruptive S content remains a further source of uncertainty. This uncertainty can be addressed using multiple scenarios before an eruption composition is known.

5.4.2 Knowledge gaps and suggestions for future research

Some large gaps remain in the regional coverage of available volatile MI data from Iceland. Of the large active volcanic systems in Iceland, there is a notable lack of data from Langjökull and Hofsjökull. Katla, one of the most productive volcanoes during the Holocene (Thordarson & Larsen 2008), has only 16 entries in the database, and the apparent exceptionally high MI S contents of the Eldgjá 934 CE eruption of Katla (Thordarson et al., 2001) warrant more research. There is also a lack of S data from Torfajökull, the largest producer of silicic magmas among active volcanoes in Iceland (Gunnarsson et al., 1998). These would all be desirable targets for future melt inclusion studies.

That the ΔS_{max} of some SIVZ melts exceed the SCSS by up to 50% is notable. This may suggest that SIVZ magmas are more oxidized than remaining Icelandic magmas and have higher proportion of dissolved S^{6+} relative to S^{2-}, which would increase the total sulfur solubility (e.g., Wallace & Edmonds 2011; Nash et al., 2019; Hughes et al., 2023). Alternatively, the high S concentration of MIs in these eruptions could be artefacts of the diffusive fractionation effect described by Baker (2008)—who observed up to 50% higher S concentrations in experimental MIs relative to matrix glasses—and would in that case relate to the MI trapping process rather than high eruptible S concentrations. To resolve the issue, more MI data from basaltic eruptions in the SIVZ, along with $S^{6+}/(S^{6+}+S^{2-})$ determinations of Icelandic glasses are needed, accompanied by directly measured SO_2 emissions of future eruptions.

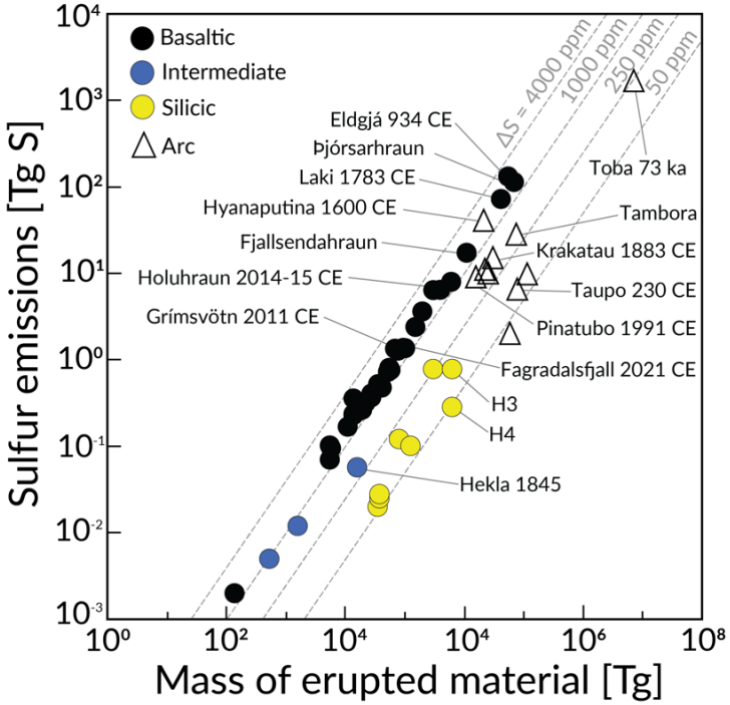

Figure 10. Sulfur emissions of Icelandic eruptions based on the petrological method. Notable arc eruptions are shown for comparison (Oppenheimer et al., 2011 and references therein). The comparison demonstrates that Icelandic eruptions typically have higher sulfur emission potentials (ΔS_{max}, dashed grey lines) than arc eruptions. The principal reason for this is that Icelandic eruptions tend to occur close to their SCSS maximum (see Fig. 8a).

6 Conclusions

This study presents an overview of volcanic S emissions of past Icelandic eruptions and the magmatic processes that control pre-eruptive S concentrations in Icelandic magmas. The results can be used for building S emission scenarios of future eruptions. The main conclusions are:

1. Compiled MI S concentrations of Icelandic eruptions show values between 10–2630 ppm and vary systematically with melt MgO and SiO_2 contents. Primitive basalts (MgO > 8wt.%) have moderate S of 400–1500 ppm. Sulfur contents increase with decreasing MgO to a peak in evolved basalts (900–2600 ppm at MgO = 4-6 wt.%; Fig. 8a). Moderate S concentrations and ΔS are observed in basaltic andesites, and lowest S and ΔS values are found in dacites and rhyolites.
2. The S/Cl ratios of Icelandic MIs are highly variable (0.5–300) but anticorrelate with indices of melt degree and source enrichment (e.g., La/Yb). A partial melting model accounting for the presence of sulfides in the mantle successfully recreates the observed S/Cl vs La/Yb trend. The data are compatible with the depleted and enriched components of the Iceland mantle having S and Cl concentrations similar to previously suggested endmembers of the MORB-source mantle (D-DMM and E-DMM).
3. Modelled SCSS and measured MI S data show similar patterns against indices of magma differentiation (FeO, MgO, SiO_2), demonstrating that pre-eruptive sulfur concentrations and hence, eruptible S content of evolving Icelandic magmas in the crust are limited by the SCSS.
4. Due to the buffering effect of mantle sulfides during melting and the limiting effect of SCSS during crustal evolution, mantle S heterogeneity and melt degree only have a minor effect on the S contents of primary melts, in contrast to other volatiles.
5. Sulfur emission potentials are highly predictable for eruptions of volcanoes that commonly erupt melts of similar major element compositions, like Grímsvötn, Bárðarbunga and the Reykjanes Peninsula volcanic systems. For volcanoes with a compositionally variable repertoire, like Hekla, the S emissions potentials are variable and multiple gas hazard scenarios must be constructed for each possible eruption type.
6. Three of the four highest sulfur emission potentials were measured in evolved basaltic eruptions from the SIVZ volcanic systems Hekla, Katla and Surtsey. This indicates that SIVZ melts may have up to 50% higher S emission potential than melts of similar compositions in other volcanic zones. However, due to scarce data for these locations, more work is needed to confirm this finding and to understand what causes the SIVZ MIs to attain S contents above apparent SCSS limits.
7. Icelandic eruptions tend to have higher S emission potentials than most volcanic eruptions globally because Icelandic melts tend to erupt at compositions where the SCSS is at its maximum.

Acknowledgements

ER thanks the national volcanic hazard assessment program for Iceland (Gosvá), funded by the National Avalanche and Landslide Fund, for generous funding that made this work possible. SAH acknowledges support from the Icelandic Research Fund (Grant #196139-051). Daniel Ben-Yehoshua and Rob Askew are thanked for bringing home and sharing samples from their Svínafellsjökull expeditions.

Data Availability Statement

The Iceland Melt Inclusion Catalogue as well as all data presented in this study and used model parameters are included in the Supplementary Information and will be made available in the online Zenodo open repository prior to the publication of the manuscript.

References

Anderson, A. T. (1974). Chlorine, sulfur, and water in magmas and oceans. *Geological Society of America Bulletin*, *85*(9), 1485-1492.

Andres, R. J., Rose, W. I., Kyle, P. R., DeSilva, S., Francis, P., & Gardeweg, M. (1991). Excessive sulfur dioxide emissions from Chilean volcanoes. *Journal of Volcanology and Geothermal Research*, *46*(3-4), 323-329.

Audétat, A., Zhang, L., & Ni, H. (2018). Copper and Li diffusion in plagioclase, pyroxenes, olivine and apatite, and consequences for the composition of melt inclusions. *Geochimica et Cosmochimica Acta*, *243*, 99-115.

Baker, D. R. (2008). The fidelity of melt inclusions as records of melt composition. *Contributions to Mineralogy and Petrology*, *156*, 377-395.

Baker, D. R., Callegaro, S., Min, A. D., Whitehouse, M. J., & Marzoli, A. (2022). Fluorine partitioning between quadrilateral clinopyroxenes and melt. *American Mineralogist*, *107*(2), 167-177.

Baker, D. R., Callegaro, S., Marzoli, A., De Min, A., Geraki, K., Whitehouse, M. J., Krzesinska, A. M., & Fioretti, A. M. (2023). Sulfur and chlorine in nakhlite clinopyroxenes: Source region concentrations and magmatic evolution. *Geochimica et Cosmochimica Acta*.

Baker, D. R., Freda, C., Brooker, R. A., & Scarlato, P. (2005). Volatile diffusion in silicate melts and its effects on melt inclusions.

Bali, E., Hartley, M. E., Halldórsson, S. A., Gudfinnsson, G. H., & Jakobsson, S. (2018). Melt inclusion constraints on volatile systematics and degassing history of the 2014–2015 Holuhraun eruption, Iceland. *Contributions to Mineralogy and Petrology*, *173*(2), 1-21.

Barsotti, S. (2020). Probabilistic hazard maps for operational use: the case of SO2 air pollution during the Holuhraun eruption (Bárðarbunga, Iceland) in 2014–2015. *Bulletin of Volcanology*, *82*(7), 1-15.

Barsotti, S., Oddsson, B., Gudmundsson, M. T., Pfeffer, M. A., Parks, M. M., Ófeigsson, B. G., et al., (2020). Operational response and hazards assessment during the 2014–2015 volcanic crisis at Bárðarbunga volcano and associated eruption at Holuhraun, Iceland. *Journal of Volcanology and Geothermal Research*, *390*, 106753.

Barsotti, S., Parks, M.M., Pfeffer, M.A., Óladóttir, B.A., Barnie, T., Titos, M.M., et al. (2023). The eruption in Fagradalsfjall (2021, Iceland): how the operational monitoring and the volcanic hazard assessment contributed to its safe access. *Natural Hazards*, *116*(3), 3063-3092.

Barth, A., & Plank, T. (2021). The Ins and Outs of Water in Olivine-Hosted Melt Inclusions: Hygrometer vs. Speedometer. *Frontiers in Earth Science*, *9*, 343.

Baxter, R. J. M., Maclennan, J., Neave, D. A., & Thordarson, T. (2023). Depth of magma storage under Iceland controlled by magma fluxes. *Geochemistry, Geophysics, Geosystems*, *24*(7), e2022GC010811.

Brounce, M., Feineman, M., LaFemina, P., & Gurenko, A. (2012). Insights into crustal assimilation by Icelandic basalts from boron isotopes in melt inclusions from the 1783–1784 Lakagígar eruption. *Geochimica et Cosmochimica Acta*, *94*, 164-180.

Bucholz, C. E., Gaetani, G. A., Behn, M. D., & Shimizu, N. (2013). Post-entrapment modification of volatiles and oxygen fugacity in olivine-hosted melt inclusions. *Earth and Planetary Science Letters*, *374*, 145-155.

Caracciolo, A., Bali, E., Guðfinnsson, G. H., Kahl, M., Halldórsson, S. A., Hartley, M. E., & Gunnarsson, H. (2020). Temporal evolution of magma and crystal mush storage conditions in the Bárðarbunga-Veiðivötn volcanic system, Iceland. *Lithos*, *352*, 105234.

Caracciolo, A., Halldórsson, S. A., Bali, E., Marshall, E. W., Jeon, H., Whitehouse, M. J., et al. (2022). Oxygen isotope evidence for progressively assimilating trans-crustal magma plumbing systems in Iceland. *Geology*, *50(7)*, *796-800*.

Caracciolo, A., Bali, E., Halldórsson, S.A., Guðfinnsson, G.H., Kahl, M., Þórðardóttir, I., et al. (2023a). Magma plumbing architectures and timescales of magmatic processes during historical magmatism on the Reykjanes Peninsula, Iceland. *Earth and Planetary Science Letters*, *621*, 118378.

Caracciolo, A., Bali, E., Ranta, E., Halldórsson, S.A., Guðfinnsson, G.H., (2023b) *Reykjanes Peninsula's historical eruptions: SO_2 emissions and future hazard implication.*EarthArXiv. https://doi.org/10.31223/X5TX05

Carboni, E., Mather, T. A., Schmidt, A., Grainger, R. G., Pfeffer, M. A., Ialongo, I., & Theys, N. (2019). Satellite-derived sulfur dioxide (SO 2) emissions from the 2014–2015 Holuhraun eruption (Iceland). *Atmospheric Chemistry and Physics*, *19*, 4851-4862.

Carlsen, H. K., Ilyinskaya, E., Baxter, P. J., Schmidt, A., Thorsteinsson, T., Pfeffer, M.A., et al., (2021). Increased respiratory morbidity associated with exposure to a mature volcanic plume from a large Icelandic fissure eruption. *Nature communications*, *12*(1), 1-12.

Carn, S. A., Fioletov, V. E., McLinden, C. A., Li, C., & Krotkov, N. A. (2017). A decade of global volcanic SO2 emissions measured from space. *Scientific reports*, *7*(1), 44095.

Danyushevsky, L. V., Della-Pasqua, F. N., & Sokolov, S. (2000). Re-equilibration of melt inclusions trapped by magnesian olivine phenocrysts from subduction-related magmas: petrological implications. *Contributions to Mineralogy and Petrology*, *138*, 68-83.

Danyushevsky, L. V., & Plechov, P. (2011). Petrolog3: Integrated software for modeling crystallization processes. *Geochemistry, Geophysics, Geosystems*, *12*(7).

Devine, J. D., Sigurdsson, H., Davis, A. N., & Self, S. (1984). Estimates of sulfur and chlorine yield to the atmosphere from volcanic eruptions and potential climatic effects. *Journal of Geophysical Research: Solid Earth*, *89*(B7), 6309-6325.

Ding, S., & Dasgupta, R. (2018). Sulfur inventory of ocean island basalt source regions constrained by modeling the fate of sulfide during decompression melting of a heterogeneous mantle. *Journal of Petrology*, *59*(7), 1281-1308.

Ding, S., Plank, T., Wallace, P. J., & Rasmussen, D. J. (2023). Sulfur_X: A model of sulfur degassing during magma ascent. *Geochemistry, Geophysics, Geosystems*, *24*(4), e2022GC010552.

Donovan, A., Pfeffer, M., Barnie, T., Sawyer, G., Roberts, T., Bergsson, B., et al. (2023). Insights into volcanic hazards and plume chemistry from multi-parameter observations: the eruptions of Fimmvörðuháls and Eyjafjallajökull (2010) and Holuhraun (2014–2015). *Natural Hazards*, 1-33

Edmonds, M., & Woods, A. W. (2018). Exsolved volatiles in magma reservoirs. *Journal of Volcanology and Geothermal Research*, *368*, 13-30.

Esse, B., Burton, M., Hayer, C., Pfeffer, M. A., Barsotti, S., Theys, N., et al. (2023). Satellite derived SO2 emissions from the relatively low-intensity, effusive 2021 eruption of Fagradalsfjall, Iceland. *Earth and Planetary Science Letters*, *619*, 118325.

Freda, C., Baker, D. R., & Scarlato, P. (2005). Sulfur diffusion in basaltic melts. *Geochimica et Cosmochimica Acta*, *69*(21), 5061-5069.

Füri, E., Hilton, D. R., Halldórsson, S. A., Barry, P. H., Hahm, D., Fischer, T. P., & Grönvold, K. (2010). Apparent decoupling of the He and Ne isotope systematics of the Icelandic mantle: The role of He depletion, melt mixing, degassing fractionation and air interaction. *Geochimica et cosmochimica acta*, *74*(11), 3307-3332.

Furman, T., Frey, F. A., & Park, K. H. (1991). Chemical constraints on the petrogenesis of mildly alkaline lavas from Vestmannaeyjar, Iceland: the Eldfell (1973) and Surtsey (1963–1967) eruptions. *Contributions to Mineralogy and Petrology*, *109*(1), 19-37.

Gaetani, G. A., O'Leary, J. A., Shimizu, N., Bucholz, C. E., & Newville, M. (2012). Rapid reequilibration of H2O and oxygen fugacity in olivine-hosted melt inclusions. *Geology*, *40*(10), 915-918.

Gaillard, F., Bouhifd, M. A., Füri, E., Malavergne, V., Marrocchi, Y., Noack, L., et al. (2021). The diverse planetary ingassing/outgassing paths produced over billions of years of magmatic activity. *Space Science Reviews*, *217*, 1-54.

Gauthier, P. J., Sigmarsson, O., Gouhier, M., Haddadi, B., & Moune, S. (2016). Elevated gas flux and trace metal degassing from the 2014–2015 fissure eruption at the Bárðarbunga volcanic system, Iceland. *Journal of Geophysical Research: Solid Earth*, *121*(3), 1610-1630.

Gerlach, T. M., & McGee, K. A. (1994). Total sulfur dioxide emissions and pre-eruption vapor-saturated magma at Mount St. Helens, 1980–88. *Geophysical Research Letters*, *21*(25), 2833-2836.

Gíslason, S. R., Stefansdottir, G., Pfeffer, M., Barsotti, S., Jóhannsson, T., Galeczka, I. M., et al. (2015). Environmental pressure from the 2014–15 eruption of Bárðarbunga volcano, Iceland. *Geochemical Perspectives Letters*, *1*(0), 84-93

Gunnarsson, B., Marsh, B.D., Taylor Jr., H.P. (1998) Generation of Icelandic rhyolites: silicic lavas from the Torfajökull central volcano. *Journal of Volcanology and Geothermal Research 83*, 1–45.

Gurenko, A. A., & Chaussidon, M. (1995). Enriched and depleted primitive melts included in olivine from Icelandic tholeiites: origin by continuous melting of a single mantle column. *Geochimica et Cosmochimica Acta*, *59*(14), 2905-2917.

Haddadi, B., Sigmarsson, O., & Larsen, G. (2017). Magma storage beneath Grímsvötn volcano, Iceland, constrained by clinopyroxene-melt thermobarometry and volatiles in melt inclusions and groundmass glass. *Journal of Geophysical Research: Solid Earth*, *122*(9), 6984-6997.

Halldórsson, S. A., Bali, E., Hartley, M. E., Neave, D. A., Peate, D. W., Guðfinnsson, G. H., et al., (2018). Petrology and geochemistry of the 2014–2015 Holuhraun eruption, central Iceland: compositional and mineralogical characteristics, temporal variability and magma storage. *Contributions to Mineralogy and Petrology*, *173*, 1-25.

Halldórsson, S. A., Barnes, J. D., Stefánsson, A., Hilton, D. R., Hauri, E. H., & Marshall, E. W. (2016a). Subducted lithosphere controls halogen enrichments in the Iceland mantle plume source. *Geology*, *44*(8), 679-682.

Halldórsson, S. A., Hilton, D. R., Barry, P. H., Füri, E., & Grönvold, K. (2016b). Recycling of crustal material by the Iceland mantle plume: new evidence from nitrogen elemental and isotope systematics of subglacial basalts. *Geochimica et Cosmochimica Acta*, *176*, 206-226.

Halldórsson, S. A., Marshall, E. W., Caracciolo, A., Matthews, S., Bali, E., Rasmussen, M. B., et al., (2022). Rapid shifting of a deep magmatic source at Fagradalsfjall volcano, Iceland. *Nature*, *609*(7927), 529-534.

Hanan, B. B., Blichert-Toft, J., Kingsley, R., & Schilling, J. G. (2000). Depleted Iceland mantle plume geochemical signature: Artifact of multicomponent mixing?. *Geochemistry, Geophysics, Geosystems*, *1*(4).

Harðardóttir, S., Halldórsson, S. A., & Hilton, D. R. (2018). Spatial distribution of helium isotopes in Icelandic geothermal fluids and volcanic materials with implications for location, upwelling and evolution of the Icelandic mantle plume. *Chemical Geology*, *480*, 12-27.

Harðardóttir, S., Matthews, S., Halldórsson, S. A., & Jackson, M. G. (2022). Spatial distribution and geochemical characterization of Icelandic mantle end-members: Implications for plume geometry and melting processes. *Chemical Geology*, *604*, 120930.

Hardarson, B. S. (1993). Alkalic rocks in Iceland, with special reference to the Snaefellsjokull volcanic system. Ph.D. thesis, University of Edinburgh, Edinburgh.

Hartley, M. E., Maclennan, J., Edmonds, M., & Thordarson, T. (2014). Reconstructing the deep CO2 degassing behaviour of large basaltic fissure eruptions. *Earth and Planetary Science Letters*, *393*, 120-131.

Hartley, M. E., Bali, E., Maclennan, J., Neave, D. A., & Halldórsson, S. A. (2018). Melt inclusion constraints on petrogenesis of the 2014–2015 Holuhraun eruption, Iceland. *Contributions to Mineralogy and Petrology*, *173*(2), 1-23.

Hartley, M., & Maclennan, J. (2018). Magmatic densities control erupted volumes in Icelandic volcanic systems. *Frontiers in Earth Science*, *6*, 29.

Hartley, M. E., De Hoog, J. C., & Shorttle, O. (2021). Boron isotopic signatures of melt inclusions from North Iceland reveal recycled material in the Icelandic mantle source. *Geochimica et Cosmochimica Acta*, *294*, 273-294.

Hauri, E. (2002). SIMS analysis of volatiles in silicate glasses, 2: isotopes and abundances in Hawaiian melt inclusions. *Chemical Geology*, *183*(1-4), 115-141.

Hauri, E. H., Maclennan, J., McKenzie, D., Gronvold, K., Oskarsson, N., & Shimizu, N. (2018). CO_2 content beneath northern Iceland and the variability of mantle carbon. *Geology*, *46*(1), 55-58.

Helgason, J. (2000, May). Geological Map of the Skaftafell Region, SE-Iceland: Glacial-Interglacial History 0-5 Ma. In *Second International Conference on Mars Polar Science and Exploration* (No. 1057, p. 71).

Helgason, Ö., Oskarsson, N., & Sigvaldason, G. E. (1992). Oxygen fugacity stratification of a magma chamber revealed by Mössbauer spectroscopy: evidence from the 1875 Askja eruption, N. Iceland. *Hyperfine Interactions*, *70*, 989-992.

Hilton, D. R., Thirlwall, M. F., Taylor, R. N., Murton, B. J., & Nichols, A. (2000). Controls on magmatic degassing along the Reykjanes Ridge with implications for the helium paradox. *Earth and Planetary Science Letters*, *183*(1-2), 43-50.

Hughes, E. C., Saper, L. M., Liggins, P., O'Neill, H. S. C., & Stolper, E. M. (2023). The sulfur solubility minimum and maximum in silicate melt. *Journal of the Geological Society*, *180*(3).

Höskuldsson, Á., Óskarsson, N., Pedersen, R., Grönvold, K., Vogfjörð, K., & Ólafsdóttir, R. (2007). The millennium eruption of Hekla in February 2000. *Bulletin of volcanology*, *70*, 169-182.

Ilyinskaya, E., Schmidt, A., Mather, T. A., Pope, F. D., Witham, C., Baxter, P., et al., (2017). Understanding the environmental impacts of large fissure eruptions: Aerosol and gas emissions from the 2014–2015 Holuhraun eruption (Iceland). *Earth and Planetary Science Letters*, *472*, 309-322.

Ito, G., Lin, J., & Gable, C. W. (1996). Dynamics of mantle flow and melting at a ridge-centered hotspot: Iceland and the Mid-Atlantic Ridge. *Earth and Planetary Science Letters*, *144*(1-2), 53-74.

Jakobsson, S. P., Pedersen, A. K., Rönsbo, J. G., & Larsen, L. M. (1973). Petrology of mugearite-hawaiite: Early extrusives in the 1973 Heimaey eruption, Iceland. *Lithos*, *6*(2), 203-214.

Jóhannesson, H., & Sæmundsson, K. (1998). Geological map of Iceland, 1: 500,000. *Tectonics. Icelandic Institute of Natural History, Reykjavik*.

Jónasson, K. (2007). Silicic volcanism in Iceland: Composition and distribution within the active volcanic zones. *Journal of Geodynamics*, *43*(1), 101-117.

Jugo, P. J., Wilke, M., & Botcharnikov, R. E. (2010). Sulfur K-edge XANES analysis of natural and synthetic basaltic glasses: Implications for S speciation and S content as function of oxygen fugacity. *Geochimica et Cosmochimica Acta*, *74*(20), 5926-5938.

Kahl, M., Bali, E., Guðfinnsson, G. H., Neave, D. A., Ubide, T., Van Der Meer, Q. H., & Matthews, S. (2021). Conditions and dynamics of magma storage in the Snæfellsnes volcanic zone, Western Iceland: insights from the Búðahraun and Berserkjahraun eruptions. *Journal of Petrology*, *62*(9), egab054.

Kern, C., Lerner, A. H., Elias, T., Nadeau, P. A., Holland, L., Kelly, P. J., et al. (2020). Quantifying gas emissions associated with the 2018 rift eruption of Kīlauea Volcano using ground-based DOAS measurements. *Bulletin of Volcanology*, *82*(7), 55

Kiseeva, E. S., & Wood, B. J. (2015). The effects of composition and temperature on chalcophile and lithophile element partitioning into magmatic sulphides. *Earth and Planetary Science Letters*, *424*, 280-294.

Korneeva, A., Kamenetsky, V. S., Nekrylov, N., Kontonikas-Charos, A., Kamenetsky, M., Savelyev, D., et al. (2023). A melt inclusion approach to reconstructing sulfur contents and sulfide saturation of primitive basaltic melts. *Lithos*, *436*, 106956

Koornneef, J. M., Stracke, A., Bourdon, B., Meier, M. A., Jochum, K. P., Stoll, B., & Grönvold, K. (2012). Melting of a two-component source beneath Iceland. *Journal of Petrology*, *53*(1), 127-157.

Kurz, M. D., Meyer, P. S., & Sigurdsson, H. (1985). Helium isotopic systematics within the neovolcanic zones of Iceland. *Earth and Planetary Science Letters*, *74*(4), 291-305.

Labidi, J., Cartigny, P., & Jackson, M. G. (2015). Multiple sulfur isotope composition of oxidized Samoan melts and the implications of a sulfur isotope 'mantle array'in chemical geodynamics. *Earth and Planetary Science Letters*, *417*, 28-39.

Larsen, G. (2002). A brief overview of eruptions from ice-covered and ice-capped volcanic systems in Iceland during the past 11 centuries: frequency, periodicity and implications. *Geological Society, London, Special Publications*, *202*(1), 81-90.

Lee, C. T. A., Luffi, P., Chin, E. J., Bouchet, R., Dasgupta, R., Morton, D. M., et al. (2012). Copper systematics in arc magmas and implications for crust-mantle differentiation. *Science*, *336*(6077), 64-68.

Lerner, A. H., Wallace, P. J., Shea, T., Mourey, A. J., Kelly, P. J., Nadeau, P. A., et al. (2021). The petrologic and degassing behavior of sulfur and other magmatic volatiles from the 2018 eruption of Kīlauea, Hawai'i: melt concentrations, magma storage depths, and magma recycling. *Bulletin of Volcanology*, *83*(6), 43.

Li, H., & Zhang, L. (2022). A thermodynamic model for sulfur content at sulfide saturation (SCSS) in hydrous silicate melts: With implications for arc magma genesis and sulfur recycling. *Geochimica et Cosmochimica Acta*, *325*, 187-204.

Liu, E. J., Cashman, K. V., Rust, A. C., & Edmonds, M. (2018). Insights into the dynamics of mafic magmatic-hydromagmatic eruptions from volatile degassing behaviour: The Hverfjall Fires, Iceland. *Journal of Volcanology and Geothermal Research*, *358*, 228-240.

Lowenstern, J.B., 1995, Applications of silicate melt inclusions to the study of magmatic volatiles. In: J.F.H. Thompson (ed). Magmas, Fluids and Ore Deposits. Mineralogical Association of Canada Short Course Volume #23, pp. 71-99.

Lucic, G., Berg, A. S., & Stix, J. (2016). Water-rich and volatile-undersaturated magmas at Hekla volcano, Iceland. *Geochemistry, Geophysics, Geosystems*, *17*(8), 3111-3130.

Maclennan, J. (2008). Concurrent mixing and cooling of melts under Iceland. *Journal of Petrology*, *49*(11), 1931-1953.

Maclennan, J. (2017). Bubble formation and decrepitation control the CO_2 content of olivine-hosted melt inclusions. *Geochemistry, Geophysics, Geosystems*, *18*(2), 597-616.

Marshall, E. W., Ranta, E., Halldórsson, S. A., Caracciolo, A., Bali, E., Jeon, H., et al., (2022). Boron isotope evidence for devolatilized and rehydrated recycled materials in the Icelandic mantle source. *Earth and Planetary Science Letters*, *577*, 117229.

Martin, E., & Sigmarsson, O. (2007). Crustal thermal state and origin of silicic magma in Iceland: the case of Torfajökull, Ljósufjöll and Snæfellsjökull volcanoes. *Contributions to Mineralogy and Petrology*, *153*, 593-605.

Mathez, E. A. (1976). Sulfur solubility and magmatic sulfides in submarine basalt glass. *Journal of Geophysical Research*, *81*(23), 4269-4276.

Matthews, S., Shorttle, O., Maclennan, J., & Rudge, J. F. (2021). The global melt inclusion C/Ba array: Mantle variability, melting process, or degassing?. *Geochimica et Cosmochimica Acta*, *293*, 525-543.

Matthews, S., Wong, K., & Gleeson, M. (2022). pyMelt: An extensible Python engine for mantle melting calculations. *Volcanica*, *5*(2), 469-475.

Métrich, N., Sigurdsson, H., Meyer, P. S., & Devine, J. D. (1991). The 1783 Lakagigar eruption in Iceland: geochemistry, CO2 and sulfur degassing. *Contributions to Mineralogy and Petrology*, *107*(4), 435-447.

Miller, W. G., Maclennan, J., Shorttle, O., Gaetani, G. A., Le Roux, V., & Klein, F. (2019). Estimating the carbon content of the deep mantle with Icelandic melt inclusions. *Earth and Planetary Science Letters*, *523*, 115699.

Momme, P., Óskarsson, N., & Keays, R. R. (2003). Platinum-group elements in the Icelandic rift system: melting processes and mantle sources beneath Iceland. *Chemical Geology*, *196*(1-4), 209-234.

1033 Moore, L. R., Gazel, E., Tuohy, R., Lloyd, A. S., Esposito, R., Steele-MacInnis, M., et al. (2015). Bubbles matter: An
1034 assessment of the contribution of vapor bubbles to melt inclusion volatile budgets. *American*
1035 *Mineralogist*, *100*(4), 806-823.
1036 Moune, S., Sigmarsson, O., Thordarson, T., & Gauthier, P. J. (2007). Recent volatile evolution in the magmatic system
1037 of Hekla volcano, Iceland. *Earth and Planetary Science Letters*, *255*(3-4), 373-389.
1038 Moune, S., Sigmarsson, O., Schiano, P., Thordarson, T., & Keiding, J. K. (2012). Melt inclusion constraints on the
1039 magma source of Eyjafjallajökull 2010 flank eruption. *Journal of Geophysical Research: Solid Earth*, *117*(B9).
1040 Nash, W. M., Smythe, D. J., & Wood, B. J. (2019). Compositional and temperature effects on sulfur speciation and
1041 solubility in silicate melts. *Earth and Planetary Science Letters*, *507*, 187-198.
1042 Neave, D. A., Bali, E., Guðfinnsson, G. H., Halldórsson, S. A., Kahl, M., Schmidt, A. S., & Holtz, F. (2019).
1043 Clinopyroxene–liquid equilibria and geothermobarometry in natural and experimental tholeiites: the 2014–2015
1044 Holuhraun eruption, Iceland. *Journal of Petrology*, *60*(8), 1653-1680.
1045 Neave, D. A., Maclennan, J., Hartley, M. E., Edmonds, M., & Thordarson, T. (2014). Crystal storage and transfer in
1046 basaltic systems: the Skuggafjöll eruption, Iceland. *Journal of Petrology*, *55*(12), 2311-2346.
1047 Neave, D. A., Hartley, M. E., Maclennan, J., Edmonds, M., & Thordarson, T. (2017a). Volatile and light lithophile
1048 elements in high-anorthite plagioclase-hosted melt inclusions from Iceland. *Geochimica et Cosmochimica Acta*,
1049 *205*, 100-118.
1050 Neave, D. A., & Putirka, K. D. (2017b). A new clinopyroxene-liquid barometer, and implications for magma storage
1051 pressures under Icelandic rift zones. *American Mineralogist*, *102*(4), 777-794.
1052 Newman, S., & Lowenstern, J. B. (2002). VolatileCalc: a silicate melt–H2O–CO2 solution model written in Visual
1053 Basic for excel. *Computers & Geosciences*, *28*(5), 597-604.
1054 Nichols, A. R. L., Carroll, M. R., & Höskuldsson, Á. (2002). Is the Iceland hot spot also wet? Evidence from the water
1055 contents of undegassed submarine and subglacial pillow basalts. *Earth and Planetary Science Letters*, 202(1),
1056 77-87.
1057 Novella, D., Maclennan, J., Shorttle, O., Prytulak, J., & Murton, B. J. (2020). A multi-proxy investigation of mantle
1058 oxygen fugacity along the Reykjanes Ridge. *Earth and Planetary Science Letters*, *531*, 115973.
1059 O'Neill, H. S. C. (2021). The thermodynamic controls on sulfide saturation in silicate melts with application to ocean
1060 floor basalts. *Magma Redox Geochemistry*, 177-213.
1061 O'Neill, H. S. C., & Mavrogenes, J. A. (2002). The sulfide capacity and the sulfur content at sulfide saturation of
1062 silicate melts at 1400 C and 1 bar. *Journal of Petrology*, *43*(6), 1049-1087.
1063 O'Neill, H. S. C., & Mavrogenes, J. A. (2022). The sulfate capacities of silicate melts. *Geochimica et Cosmochimica*
1064 *Acta*, *334*, 368-382.
1065 Oppenheimer, C., Scaillet, B., & Martin, R. S. (2011). Sulfur degassing from volcanoes: source conditions,
1066 surveillance, plume chemistry and earth system impacts. *Reviews in Mineralogy and Geochemistry*, *73*(1), 363-
1067 421.
1068 Óskarsson N, Grönvold K, Larsen G (1984) The haze produced by the Laki eruption. In Einarsson T, Gudbergsson
1069 GM, Gunnlaugsson GA, Rafnsson S, Thorarinsson S (eds) Skaftáreldar 1783–1784: Ritgerdir og Heimildir. Mál
1070 og Menning, Reykjavík, pp 67–80
1071 Óskarsson, N., Helgason, Ö., & Steinthórsson, S. (1994). Oxidation state of iron in mantle-derived magmas of the
1072 Icelandic rift zone. *Hyperfine Interactions*, *91*, 733-737.
1073 Owen, J., Tuffen, H., & McGarvie, D. W. (2013). Using dissolved H2O in rhyolitic glasses to estimate palaeo-ice
1074 thickness during a subglacial eruption at Bláhnúkur (Torfajökull, Iceland). *Bulletin of volcanology*, *74*(6), 1355-
1075 1378.
1076 Padilla, A. J., Miller, C. F., Carley, T. L., Economos, R. C., Schmitt, A. K., Coble, M. A., et al., (2016). Elucidating
1077 the magmatic history of the Austurhorn silicic intrusive complex (southeast Iceland) using zircon elemental and
1078 isotopic geochemistry and geochronology. *Contributions to Mineralogy and Petrology*, *171*, 69.
1079 Palais, J.M., & Sigurdsson, H. (1989). Petrologic evidence of volatile emissions from major historic and pre-historic
1080 volcanic eruptions. *Understanding Climate Change, Geophys. Monogr*. Ser, *52*, 31-53.
1081 Pedersen, G. B., Belart, J. M., Óskarsson, B. V., Gudmundsson, M. T., Gies, N., Högnadóttir, T., et al. (2022). Volume,
1082 effusion rate, and lava transport during the 2021 Fagradalsfjall eruption: Results from near real-time
1083 photogrammetric monitoring. *Geophysical Research Letters*, *49*(13), e2021GL097125.
1084 Pedersen, G. B. M., Höskuldsson, A., Dürig, T., Thordarson, T., Jonsdottir, I., Riishuus, M. S., et al. (2017). Lava
1085 field evolution and emplacement dynamics of the 2014–2015 basaltic fissure eruption at Holuhraun,
1086 Iceland. *Journal of Volcanology and Geothermal Research*, *340*, 155-169.
1087 Pfeffer, M. A., Arellano, S., Barsotti, S., Petersen, G. N., Barnie, T., Ilyinskaya, E., et al. (in review). SO_2 emission
1088 rates and incorporation into the air pollution dispersion forecast during the 2021 eruption of Fagradalsfjall,
1089 Iceland. Submitted to Journal of Volcanology and Geothermal Research.

Pfeffer, M. A., Bergsson, B., Barsotti, S., Stefánsdóttir, G., Galle, B., Arellano, S., et al. (2018). Ground-based measurements of the 2014–2015 Holuhraun volcanic cloud (Iceland). *Geosciences*, *8*(1), 29.

Plank, T., Kelley, K. A., Zimmer, M. M., Hauri, E. H., & Wallace, P. J. (2013). Why do mafic arc magmas contain∼ 4 wt.% water on average?. *Earth and Planetary Science Letters*, *364*, 168-179.

Poreda, R., Schilling, J. G., & Craig, H. (1986). Helium and hydrogen isotopes in ocean-ridge basalts north and south of Iceland. *Earth and Planetary Science Letters*, *78*(1), 1-17.

Portnyagin, M., Hoernle, K., Storm, S., Mironov, N., van den Bogaard, C., & Botcharnikov, R. (2012). H_2O-rich melt inclusions in fayalitic olivine from Hekla volcano: Implications for phase relationships in silicic systems and driving forces of explosive volcanism on Iceland. *Earth and Planetary Science Letters*, *357*, 337-346.

Ranta, E. (2022). Stable isotopes of volatile elements as a window into the crust and mantle beneath Icelandic volcanoes. PhD thesis, University of Iceland, pp. 201.

Ranta, E., Gunnarsson-Robin, J., Halldórsson, S. A., Ono, S., Izon, G., Jackson, M. G., et al. (2022). Ancient and recycled sulfur sampled by the Iceland mantle plume. *Earth and Planetary Science Letters*, *584*, 117452.

Ranta, E. J., Halldórsson, S. A., Barnes, J. D., Jónasson, K., & Stefánsson, A. (2021). Chlorine isotope ratios record magmatic brine assimilation during rhyolite genesis. *Geochemical Perspectives Letters* 16, 35–39.

Ranta, E., Halldórsson, S.A., Barry, P.H., Ono, S., Gunnarsson Robin, J.G., Kleine, B.I., et al. (2023). Deep magma degassing and volatile fluxes through volcanic hydrothermal systems: Insights from the Askja and Kverkfjöll volcanoes, Iceland. *Journal of Volcanology and Geothermal Research*, *436*, 107776.

Rasmussen, D. J., Plank, T. A., Wallace, P. J., Newcombe, M. E., & Lowenstern, J. B. (2020). Vapor-bubble growth in olivine-hosted melt inclusions. *American Mineralogist: Journal of Earth and Planetary Materials*, *105*(12), 1898-1919.

Reekie, C. D. J., Jenner, F. E., Smythe, D. J., Hauri, E. H., Bullock, E. S., & Williams, H. M. (2019). Sulfide resorption during crustal ascent and degassing of oceanic plateau basalts. *Nature communications*, *10*(1), 82.

Robock, A. (2000). Volcanic eruptions and climate. Reviews of geophysics, *38*(2), 191-219.

Rooyakkers, S. M., Stix, J., Berlo, K., Petrelli, M., Hampton, R. L., Barker, S. J., & Morgavi, D. (2021). The origin of rhyolitic magmas at Krafla Central Volcano (Iceland). *Journal of Petrology*, *62*(8), egab064.

Rottier, B., & Audétat, A. (2019). In-situ quantification of chlorine and sulfur in glasses, minerals and melt inclusions by LA-ICP-MS. *Chemical Geology*, *504*, 1-13.

Scaillet, B., Luhr, J., & Carroll, M. R. (2003a). Petrological and volcanological constraints on volcanic sulfur emissions to the atmosphere. *Geophysical Monograph - American Geophysical Union*, *139*, 11-40.

Scaillet, B., & Pichavant, M. (2003b). Experimental constraints on volatile abundances in arc magmas and their implications for degassing processes. *Geological Society, London, Special Publications*, *213*(1), 23-52.

Schattel, N., Portnyagin, M., Golowin, R., Hoernle, K., & Bindeman, I. (2014). Contrasting conditions of rift and off-rift silicic magma origin on Iceland. *Geophysical Research Letters*, *41*(16), 5813-5820.

Schiavi, F., Bolfan-Casanova, N., Buso, R., Laumonier, M., Laporte, D., Medjoubi, K., et al. (2020). Quantifying magmatic volatiles by Raman microtomography of glass inclusion-hosted bubbles. *Geochemical Perspectives Letters*, *16*, 17-24.

Schilling, J. G. (1973). Iceland mantle plume: geochemical study of Reykjanes Ridge. *Nature*, *242*(5400), 565-571.

Schipper, C. I., Le Voyer, M., Moussallam, Y., White, J. D., Thordarson, T., Kimura, J. I., & Chang, Q. (2016). Degassing and magma mixing during the eruption of Surtsey Volcano (Iceland, 1963–1967): the signatures of a dynamic and discrete rift propagation event. *Bulletin of Volcanology*, *78*(4), 1-19.

Schmidt, A., Ostro, B., Carslaw, K. S., Wilson, M., Thordarson, T., Mann, G. W., & Simmons, A. J. (2011). Excess mortality in Europe following a future Laki-style Icelandic eruption. *Proceedings of the National Academy of Sciences*, *108*(38), 15710-15715.

Schmidt, A., Leadbetter, S., Theys, N., Carboni, E., Witham, C. S., Stevenson, J. A., et al. (2015). Satellite detection, long-range transport, and air quality impacts of volcanic sulfur dioxide from the 2014–2015 flood lava eruption at Bárðarbunga (Iceland). *Journal of Geophysical Research: Atmospheres*, *120*, 9739-9757.

Scott, S., Pfeffer, M., Oppenheimer, C., Bali, E., Lamb, O. D., Barnie, T., et al. (2023). Near-surface magma flow instability drives cyclic lava fountaining at Fagradalsfjall, Iceland. *Nature Communications*, *14*, 6810.

Sharma, K., Blake, S., Self, S., & Krueger, A. J. (2004). SO_2 emissions from basaltic eruptions, and the excess sulfur issue. *Geophysical Research Letters*, *31*(13).

Sharma, K., Self, S., Blake, S., Thordarson, T., & Larsen, G. (2008). The AD 1362 Öræfajökull eruption, SE Iceland: Physical volcanology and volatile release. *Journal of Volcanology and Geothermal Research*, *178*(4), 719-739.

Shima, H., & Naldrett, A. J. (1975). Solubility of sulfur in an ultramafic melt and the relevance of the system Fe-SO. *Economic Geology*, *70*(5), 960-967.

Shimizu, K., Saal, A. E., Myers, C. E., Nagle, A. N., Hauri, E. H., Forsyth, D. W., et al. (2016). Two-component mantle melting-mixing model for the generation of mid-ocean ridge basalts: Implications for the volatile content of the Pacific upper mantle. *Geochimica et Cosmochimica Acta*, *176*, 44-80.

1148 Shinohara, H. (2008). Excess degassing from volcanoes and its role on eruptive and intrusive activity. *Reviews of*
1149 *Geophysics*, *46*(4).
1150 Shorttle, O., & Maclennan, J. (2011). Compositional trends of Icelandic basalts: Implications for short–length scale
1151 lithological heterogeneity in mantle plumes. *Geochemistry, Geophysics, Geosystems*, *12*(11).
1152 Shorttle, O., Maclennan, J., & Lambart, S. (2014). Quantifying lithological variability in the mantle. *Earth and*
1153 *Planetary Science Letters*, *395*, 24-40.
1154 Sigmarsson, O., Haddadi, B., Carn, S., Moune, S., Gudnason, J., Yang, K., & Clarisse, L. (2013). The sulfur budget
1155 of the 2011 Grímsvötn eruption, Iceland. *Geophysical Research Letters*, *40*(23), 6095-6100.
1156 Sigmarsson, O., & Halldórsson, S. A. (2015). Delimiting Bárðarbunga and Askja volcanic systems with Sr-and Nd-
1157 isotope ratios. *Jökull*, *65*, 17-27.
1158 Sigmarsson, O., Moune, S., & Gauthier, P. J. (2020). Fractional degassing of S, Cl and F from basalt magma in the
1159 Bárðarbunga rift zone, Iceland. *Bulletin of Volcanology*, *82*(7), 1-8.
1160 Sigmundsson, F., Pinel, V., Grapenthin, R., Hooper, A., Halldórsson, S. A., Einarsson, P., et al. (2020). Unexpected
1161 large eruptions from buoyant magma bodies within viscoelastic crust. *Nature communications*, *11*(1), 2403.
1162 Sigurdsson H (1982) Volcanic pollution and climate: the 1783 Laki eruption. *EOS*, *63*, 601–602
1163 Sigvaldason, G. E., & Óskarsson, N. (1976). Chlorine in basalts from Iceland. *Geochimica et Cosmochimica*
1164 *Acta*, *40*(7), 777-789.
1165 Simmons, I. C., Pfeffer, M. A., Calder, E. S., Galle, B., Arellano, S., Coppola, D., & Barsotti, S. (2017). Extended
1166 SO_2 outgassing from the 2014–2015 Holuhraun lava flow field, Iceland. *Bulletin of Volcanology*, *79*(11), 1-11.
1167 Smythe, D. J., Wood, B. J., & Kiseeva, E. S. (2017). The S content of silicate melts at sulfide saturation: new
1168 experiments and a model incorporating the effects of sulfide composition. *American Mineralogist*, *102*(4), 795-
1169 803.
1170 Stefánsson, A., Stefánsdóttir, G., Keller, N. S., Barsotti, S., Sigurdsson, Á., Thorláksdóttir, S. B., et al., (2017). Major
1171 impact of volcanic gases on the chemical composition of precipitation in Iceland during the 2014–2015
1172 Holuhraun eruption. *Journal of Geophysical Research: Atmospheres*, *122*(3), 1971-1982.
1173 Stewart, C., Damby, D. E., Horwell, C. J., Elias, T., Ilyinskaya, E., Tomašek, I., et al., (2022). Volcanic air pollution
1174 and human health: recent advances and future directions. *Bulletin of Volcanology*, *84*(1), 1-25.
1175 Su, Y., Huber, C., Bachmann, O., Zajacz, Z., Wright, H., & Vazquez, J. (2016). The role of crystallization-driven
1176 exsolution on the sulfur mass balance in volcanic arc magmas. *Journal of Geophysical Research: Solid Earth*,
1177 *121*(8), 5624-5640.
1178 Thomson, A., & Maclennan, J. (2013). The distribution of olivine compositions in Icelandic basalts and
1179 picrites. *Journal of Petrology*, *54*(4), 745-768.
1180 Thordarson, T., & Larsen, G. (2007). Volcanism in Iceland in historical time: Volcano types, eruption styles and
1181 eruptive history. *Journal of Geodynamics*, *43*(1), 118-152.
1182 Thordarson, T., Miller, D. J., Larsen, G., Self, S., & Sigurdsson, H. (2001). New estimates of sulfur degassing and
1183 atmospheric mass-loading by the 934 AD Eldgjá eruption, Iceland. *Journal of Volcanology and Geothermal*
1184 *Research*, *108*(1-4), 33-54.
1185 Thordarson, T., Self, S., Miller, D. J., Larsen, G., & Vilmundardóttir, E. G. (2003). Sulphur release from flood lava
1186 eruptions in the Veidivötn, Grímsvötn and Katla volcanic systems, Iceland. *Geological Society, London, Special*
1187 *Publications*, *213*(1), 103-121.
1188 Thordarson, T., Self, S., Oskarsson, N., & Hulsebosch, T. (1996). Sulfur, chlorine, and fluorine degassing and
1189 atmospheric loading by the 1783–1784 AD Laki (Skaftár Fires) eruption in Iceland. *Bulletin of Volcanology*, *58*,
1190 205-225.
1191 Þórðardóttir, I. (2020). A microprobe study of tephra glasses from the Fjallsendahraun lava, central Iceland (BSc
1192 Thesis, University of Iceland).
1193 van der Meer, Q. H., Bali, E., Guðfinnsson, G. H., Kahl, M., & Rasmussen, M. B. (2021). Warm and slightly reduced
1194 mantle under the off-rift Snæfellsnes Volcanic Zone, Iceland. *Journal of Petrology*, *62*(12), egab057.
1195 Wallace, P. J., & Edmonds, M. (2011). The sulfur budget in magmas: evidence from melt inclusions, submarine
1196 glasses, and volcanic gas emissions. *Reviews in Mineralogy and Geochemistry*, *73*(1), 215-246.
1197 Watkins, J. M., Gardner, J. E., & Befus, K. S. (2017). Nonequilibrium degassing, regassing, and vapor fluxing in
1198 magmatic feeder systems. *Geology*, *45*(2), 183-186.
1199 Venugopal, S., Schiavi, F., Moune, S., Bolfan-Casanova, N., Druitt, T., & Williams-Jones, G. (2020). Melt inclusion
1200 vapour bubbles: the hidden reservoir for major and volatile elements. *Scientific Reports*, *10*(1), 9034.
1201 Wieser, P. & Gleeson, M. (2023). PySulfSat: An open-source Python3 tool for modeling sulfide and sulfate saturation.
1202 *Volcanica*, *6*(1), 107–127. doi: 10.30909/vol.06.01.107127.
1203 Wieser, P. E., Jenner, F., Edmonds, M., Maclennan, J., & Kunz, B. E. (2020). Chalcophile elements track the fate of
1204 sulfur at Kīlauea Volcano, Hawai'i. *Geochimica et Cosmochimica Acta*, *282*, 245-275.

Vignelles, D., Roberts, T. J., Carboni, E., Ilyinskaya, E., Pfeffer, M., Waldhauserova, P. D., et al. (2016). Balloon-borne measurement of the aerosol size distribution from an Icelandic flood basalt eruption. *Earth and Planetary Science Letters*, *453*, 252-259.

Wolfe, C. J., Th. Bjarnason, I., VanDecar, J. C., & Solomon, S. C. (1997). Seismic structure of the Iceland mantle plume. *Nature*, *385*(6613), 245-247.

Workman, R. K., & Hart, S. R. (2005). Major and trace element composition of the depleted MORB mantle (DMM). *Earth and Planetary Science Letters*, *231*(1-2), 5.